# Upper Ordovician stratigraphy of the Stora Sutarve core (Gotland, Sweden) and an assessment of the Hirnantian Isotope Carbon Excursion (HICE) in high-resolution

***Niklas Gunnarsson***

**Dissertations in Geology at Lund University,**
**Master's thesis, no 649**
**(45 hp/ECTS credits)**

**Department of Geology**
**Lund University**
**2023**

# Upper Ordovician stratigraphy of the Stora Sutarve core (Gotland, Sweden) and an assessment of the Hirnantian Isotope Carbon Excursion (HICE) in high-resolution

Master's thesis

Niklas Gunnarsson

Department of Geology
Lund University
2023

# Contents



**Cover Picture:** Thin section from the Loka Formation showing conspicuously laminated grainstone-packstone sets separated by thin lamina of organic-rich mudstone. The skeletal fragments are mainly derived from crinoids. Note concentric laminated ooid in the lower middle part of the photograph. Photo: Niklas Gunnarsson

# Upper Ordovician stratigraphy of the Stora Sutarve core (Gotland, Sweden) and an assessment of the Hirnantian Isotope Carbon Excursion (HICE) in high-resolution

Niklas Gunnarsson

Gunnarsson, N., 2023: Upper Ordovician stratigraphy of the Stora Sutarve core (Gotland, Sweden) and an assessment of the Hirnantian Isotope Carbon Excursion (HICE) in high-resolution. *Dissertations in Geology at Lund University*, No. 649, 33 pp. 45 hp (45 ECTS credits).

**Abstract:** The Hirnantian Isotope Carbon Excursion (HICE) is a major anomaly in Earths global carbon cycle at the end of the Ordovician time period, at ca 445 Ma. The anomaly is intimately associated with substantial cooling of the global climate, expansion of continental ice-sheets and the Late Ordovician Mass Extinction (LOME). The present study investigates the Upper Ordovician to the lowermost Silurian sedimentary record, with particular emphasis on carbonate microfacies and carbon isotope stratigraphy of the Hirnantian Stage, based on the recently drilled Stora Sutarve core from southern Gotland. The lithological record has similarities with both the East Baltic and Swedish successions and includes the Kahula (including 13 bentonites), Hirmuse, Rägavere, Paekna, Jonstorp, Loka, Motala and Kallholn formations and spans the Sandbian to the Aeronian stages. Several δ13C excursions have been identified in the core; LSNICE, GICE, Moe excursion, HICE and possibly the Late Aeronian CIE. The Hirnantian Stage and the HICE is entirely confined to the Loka Formation in the core. The Loka Formation constitutes a lower limestone unit (Skultorp Member) overlain by a more argillaceous unit (informal 'upper member'). Both units yield abundant brachiopods of both the Hirnantia and Edgewood-Cathay faunas. This formation is interpreted as one cycle of transgression-regression bounded by hiatuses at the lower and upper boundary, inferably glacially induced. The HICE includes a slowly increasing rising limb, a peak and plateau, which is truncated at an unconformity at the upper boundary of the Loka Formation. Based on the dense sampling four clusters of δ13C values help to define significant changes in the HICE trend that may facilitate global correlation of the succession and the herein interpreted sea-level change.

**Keywords:** *Hirnantia* fauna, carbon isotope stratigraphy, Hirnantian, Baltoscandian basin, Loka Formation, Upper Ordovician, Sweden

**Supervisor:** Mikael Calner

**Subject:** Bedrock Geology

*Niklas Gunnarsson, Department of Geology, Lund University, Sölvegatan 12, SE-223 62 Lund, Sweden. E-mail: niklas.gunnarsson@protonmail.com*

# Övre ordovicisk stratigrafi från Stora Sutarve kärnan (Gotland) och en högupplöst studie av Hirnantian Isotope Carbon Excursion (HICE)

Niklas Gunnarsson

Gunnarsson, N., 2023: Övre ordovicisk stratigrafi från Stora Sutarve kärnan (Gotland) och en högupplöst studie av Hirnantian Isotope Carbon Excursion (HICE). *Examensarbeten i geologi vid Lunds universitet*, Nr. 649, 33 sid. 45 hp.

**Sammanfattning:** En avsevärd anomali i jordens globala kolcykel, känd som Hirnantian Isotope Carbon Excursion (HICE), finns dokumenterad i lagerföljder från Hirnantetagen, i slutet av Ordovicium för cirka 445 miljoner år sedan. Anomalin är kopplad till den samtida globala nedkylningen, bildande av inlandisar och ett massutdöende – Late Ordovician Mass Extinction (LOME). Denna studie undersöker lagerföljder från övre Ordovicium till lägre Silur i en nyligen upptagen borrkärna från södra Gotland. Särskild vikt läggs på beskrivning av kalkstenen och kolisotopstratigrafin i Hirnant-etagen. Borrkärnans lagerföljd har likheter med såväl baltiska som svenska lagerföljder och inkluderar Kahula (inklusive 13 bentoniter), Hirmuse, Rägavere, Paekna, Jonstorp, Loka, Motala och Kallholn formationerna och sträcker sig från Sandby-etagen till Aeron-etagen. Flera δ13C-anomalier har identifierats i kärnan; LSNICE, GICE, Moe-anomalin, HICE och med viss osäkerhet den sen-Aeronska CIE. Hirnant-etagen och HICE är begränsad inom Lokaformationen i borrkärnan. Loka formationen består av en lägre kalkstensenhet (Skultorpledet) och en övre enhet med högre lerhalt (ej formellt namngiven). Båda enheterna innehåller brachiopoder av Hirnantia- och Edgewood-Cathay faunan. Formationen tolkas som en lagerföljd avsatt i en transgression-regressionscykel med glacialt formade erosionsytor i formationens nedre och övre gräns. HICE består av en långsamt uppgående trend följt av en topp och platå. Platån är trunkerad vid en erosionsyta vid formationens övre gräns. Den täta provtagningen tydliggör fyra trender i kluster av δ13C-värden. Klusterna framhäver signifikanta förändringar i HICE, som kan underlätta global korrelation av lagerföljder och havsnivåtolkningarna i denna studie.

**Nyckelord:** Hirnantia fauna, kolisotoper, Hirnant-etagen, Baltoskandiska bassängen, Lokaformationen, Övre ordovicium, Sverige

**Handledare**: Mikael Calner

**Ämnesinriktning**: Berggrundsgeologi

*Niklas Gunnarsson, Geologiska institutionen, Lunds Universitet, Sölvegatan 12, 223 62 Lund, Sverige. E-post: niklas.gunnarsson@protonmail.com*

# 1 Introduction

## 1.1 The Hirnantian Stage

The Hirnantian Stage of the latest Ordovician is associated with major changes in the global environment and marine biodiversity. The environmental changes were related to glaciation on Gondwana during the Early Paleozoic Icehouse (EPI; Page et al., 2007) which eventually led to the second largest mass extinction in Earth's history, the Late Ordovician Mass Extinction (LOME; Harper et al., 2014; Rong et al., 2020; Sheehan, 2001; Zou et al., 2018). Intimately associated with the environmental changes and the LOME is a major anomaly in the global carbon cycle (as measured by $\delta^{13}C$) known as the Hirnantian Isotope Carbon Excursion (HICE; Bergström, Lehnert, et al., 2012; Brenchley, 2004; Calner et al., 2021). In terms of duration the Hirnantian Stage is brief, ranging from 445.21 – 443.07 Ma (Gradstein et al. 2020). A duration somewhere between 1.3 – 2 Ma has been repeated in several studies. It should be noted, however, that the recent study of Ling et al. (2019) suggest that the stage may be contained within a time span as brief as 0.47 +/- 0.34 Ma, between 443.14 Ma and 442.67 Ma according to U-Pb dating of K-bentonite in a continuous section in China.

The EPI represents a cool period beginning in the Late Ordovician and extending into the Early Silurian, with several glacial maxima and perturbation in the carbon cycle (Page et al., 2007). Paradoxically the Late Ordovician had much greater $pCO_2$ levels than present day (Berner, 1990) and it is not fully clear how ice-sheets could expand through to the extent they did in this situation. It may be explained by the palaeogeographic configuration, with much of the landmass concentrated close to the South Pole, along with a decreased solar luminosity (Crowley & Baum, 1991; Pohl et al., 2014; Poussart et al., 1999). The cooling in the Late Ordovician may have been caused by weathering of a large igneous province, formed in the Katian (Lefebvre et al., 2010; Longman et al., 2021) or of mountains formed during the Taconic orogeny (Kump et al., 1999). Increased primary production and organic burial that led to a substantial decrease in atmospheric $pCO_2$ has also been suggested as the driving mechanism behind the global cooling (Brenchley et al., 1994). Orbital configuration likely had an effect on the Late Ordovician climate and may have set up the conditions required for a glaciation (Poussart et al., 1999; Williams, 1991).

The Hirnantian Stage marks the time of greatest ice extent during the EPI (Page et al., 2007) and may comprise two pulses of ice-sheet growth (Sutcliffe et al., 2000). In several outcrops with glacigenic rocks, in both northern and southern Africa, the two pulses are mirrored as subglacial erosion surfaces with glacial retreat strata above (Sutcliffe et al., 2000). The full Hirnantian glacial with its two pulses, is largely contained within the *Normalograptus extraordinarius* graptolite biozone (Harper et al., 2014; Wang et al., 2019), which lasted ca 0.2 Ma (Ling et al., 2019; Sutcliffe et al., 2000). The timing of the pulses suggests they may be controlled by eccentricity cycles (Sutcliffe et al., 2000). The post-glacial sea level rise occurred in the *Normalograptus perscultpus* graptolite biozone (Harper et al., 2014; Sutcliffe et al., 2000; Wang et al., 2019).

Ghienne et al. (2014) identified three regression -transgression cycles named Late Ordovician Glacial Cycles 1-3 (LOGC 1-3). The first cycle, LOGC-1, occurred in the latest Katian and includes a regression and a transgression due to ice-sheet growth and decline (Ghienne et al., 2014). LOGC-2 includes a similar cycle and corresponds to the *Belonechitina gamachiana* chitinozoan biozone, which Ghienne et al. (2014) includes in the Hirnantian Stage. The regression in the last cycle, LOGC 3, represent the most extensive ice-sheet growth, whereas the ensuing transgression reflects the post-glacial sea-level rise, which extended into the Silurian (Ghienne et al., 2014). It should be noted that this interpretation extends the Hirnantian Stage to include the *Belonechitina gamachiana* chitinozoan biozone (Ghienne et al., 2014) in opposition to the interpretation in Baltica where *Belonechitina gamachiana* belongs in the Katian Stage (see Calner et al. 2021).

The cool climate during the EPI eventually led to the first of the big five mass extinction events (Berry et al., 1995), with a calculated total loss of 85% of the marine species (Jablonski, 1991). The extinction can be divided into two pulses, in the Hirnantian Stage, the first pulse in the *Normalograptus extraordinarius* graptolite biozone and the second pulse in the *Normalograptus perscultpus* graptolite biozone (Brenchley et al., 2003; Harper et al., 2014; Sheehan, 2001). The first pulse is connected to the initiation of the glacial although the exact killing mechanism is unclear (Harper et al., 2014). Several factors, such as euxinia and anoxia in the water column combined with substantial global lowering of the sea level, played a role in the first extinction pulse (Hammarlund et al., 2012; Harper et al., 2014). At the end of the glacial, in the *persculptus* graptolite biozone, sea-level rose again, anoxia became widespread (Hammarlund et al., 2012) and a second cycle of euxinia occurred (Zou et al., 2018), which led to the second extinction pulse.

The *Hirnantia* brachiopod Fauna is a characteristic marker for the Hirnantian Stage as it not only survived the first extinction pulse but adapted and expanded to become abundant in the cool climate (Rong et al., 2020; Wang et al., 2019). This fauna was, however, overall short lived and became extinct during the second extinction pulse due to anoxia and euxinia associated with the post-glacial warming (Harper et al., 2014; Rong et al., 2020). Post glaciation, the sea was repopulated with fauna thriving in a warming climate, among these the Edgewood-Cathay brachiopod fauna (Rong et al., 2020). Thus these two brachiopod faunas appear consecutively in strata, respectively, after the first and second extinction pulse, during glaciations and post glaciation (Rong et al., 2020). The overall benthic fauna of the Hirnantian has been further subdivided into three 'transitional benthic faunas' (TBF), with focus on brachiopod assemblages and also the presence of corals and sponges (Wang et al., 2019). TBF-1 is associated with the majority of species of the cool climate *Hirnantia* fauna, which was spread from the temperate to tropic regions, inhabiting a variety of water depths. TBF-2 is associated with warmer water

and is characterized by brachiopods such as *Hindella* and *Dalmanella* without key members of the Hirnantian fauna present. Rugose corals are also associated with TBF-2. It is stratigraphically above the TBF-1, in the middle Hirnantian. TBF-2 occurs at most latitudes and is replaced by sponges in deeper offshore waters. TBF-3, which constitutes the Edgewood brachiopod fauna and the *Cathayisiorthis* brachiopod fauna, replaces and is stratigraphically above TBF-2 in later Hirnantian. Rugose and tabulate corals are also associated with TBF-3. This fauna is, in similarity with TBF-2, associated with warm water and occurs at most latitude and is replaced by sponges in deeper offshore waters (Wang et al., 2019). Based on the absence of cold water fauna in the late Hirnantian Wang et al. (2019) suggested a major glaciation in the Katian-Hirnantian transition, associated with TBF-1, followed by deglaciation associated with TBF-2 and TBF-3. Within the deglaciation two minor glaciations were inferred.

## 1.2 The Hirnantian Isotope Carbon Excursion

The Late Ordovician hosts a series of anomalies in the $\delta^{13}C$ record of marine carbonates. These anomalies are mostly well constrained by biostratigraphy and also identified in several remote locations. They can thus be interpreted as reflecting offsets or disruptions to the global carbon cycle and related to climate change. The Guttenberg Isotope Carbon Excursion (GICE) and the Hirnantian Isotope Carbon Excursion (HICE) are recognized as global excursions (Ainsaar et al., 2010). In the Baltoscandian basin, and especially based on stratigraphic sections in the East Baltic area, the Rakvere, Saunja, Moe and Paroveja carbon isotope excursions (Fig. 1) have been identified (Ainsaar et al., 2010). Uncertainty remains how these smaller excursions relate to the North American Kope, Fairview, Waynesville, Whitewater and Elkhorn excursions (Ainsaar et al., 2010; Bergström et al., 2010; Gradstein et al., 2020). In the Baltoscandian basin, the Lower Sandbian Negative Isotope Carbon Excursion (LSNICE) has also been identified (Bauert et al., 2014; Bergström, Schmitz, et al., 2020). The HICE is the most profound of all Ordovician anomalies in terms of offset from baseline values and is known from many tens of localities globally (Achab et al., 2011; Ainsaar et al., 2010; Bergström, Lehnert, et al., 2012; Bergström et al., 2014; Brenchley et al., 2003; Calner et al., 2021; Chen et al., 2006; Ebbestad et al., 2015; Fan et al., 2009; Finney et al., 1999; Jones et al., 2011; Ripperdan et al., 1998) and therefore represents an exceptional geochemical marker for correlations of even thin packages of sedimentary strata between regions and continents. A stratigraphic problem however is that the base of the Hirnantian corresponds to the first appearance datum of the chitinozoan *S. taugourdeuai* in Northern Europe (Kiipli & Kiipli, 2020), whereas the base is defined by the chitinozoan *Belonechitina gamachiana* in North America (Amberg et al., 2016; see Calner et al., 2021 for a discussion). The rise and fall of the HICE is contemporaneous with the rise and fall of $\delta^{18}O$ values and sea-level changes caused by the growth and decline of ice-sheet on Gondwana (Brenchley et al., 2003). From a morphological point of view, the ideal tripartite signature of the HICE consists of a rising limb, a peak interval (sometimes extended as a plateau), and a falling limb, as first discussed from East Baltic cores by Brenchley et al., (2003). The rising limb and the falling limb reflect the onset of glaciation and the final post-glacial sea level rise, respectively (Brenchley et al., 2003). The truncation of the falling limb seen in both Baltoscandia and North America infers a stratigraphic gap in these successions (Brenchley et al., 2003). The range in $\delta^{13}C$ (‰) of the truncation may reflect position on the ramp, as cores from higher up on the ramp display a greater drop of $\delta^{13}C$ (Brenchley et al., 2003).

The exact cause and mechanism of the increased $\delta^{13}C$ values during the Hirnantian remains unknown. The above mentioned productivity hypothesis as the cause of the global cooling (Brenchley et al., 1994) offers carbon burial as an explanation.

## 1.3 The Hirnantian Stage in Baltoscandia

The preserved sedimentary record of the Hirnantian Stage in southern Sweden is generally only a few meters thick and is represented by different formations in different geographical areas (Fig. 1). In Scania the Hirnantian Stage includes mainly mudrock and shale belonging to the Lindegård Mudstone and Kallholn Formation (Bergström et al., 2014). In the Siljan region the Hirnantian Stage is included in parts of the carbonate mud mounds of the Boda Limestone and the overlying Glisstjärn Formation (Schmitz & Bergström, 2007). At the Råssnäsudden outrop, near the city of Motala, the Hirnantian Stage is confined within the Loka Formation, which was established and defined by Bergström and Bergström (1996). This name has replaced the previous formation names Tommarp Formation (Jaanusson, 1982) and Dalmanitina Beds. At Råssnäsudden, the formation constitutes a lower unit of mudrock, a middle unit of oolitic limestone and an upper unit of mudrock (Bergström & Bergström, 1996). The corresponding succession can be studied in the now well-studied Borenshult drillcore, which was drilled in the city of Motala, near the outcrop where the Loka Formation was established (Bergström et al., 2011). In the Borenshult core, the total Hirnantian is 3.86 m thick and the lower member of the Loka Formation is missing (Bergström et al., 2011). Here the formation starts with a quartz-rich oolitic and laminated grainstone (Skultorp Member), overlain by a calcareous mudstone, and the upper and lower boundaries of the formation is developed as unconformities (Bergström et al., 2011). The Skultorp Member was originally studied and described from Mösseberg in Västergötland by Stridsberg (1980) who characterized it as a warm water oolitic and coral bearing limestone. The δ13C values of the HICE of Borenshult show a rapid rise from baseline values around +1‰ to peak values between +3‰ and + 4‰ in the oolitic Skultorp Member, then a drop to values which fluctuate around +2‰ in the informal ‘upper member’, followed by a drop to baseline values at ca +0.5‰ (Bergström, Lehnert, et al., 2012).

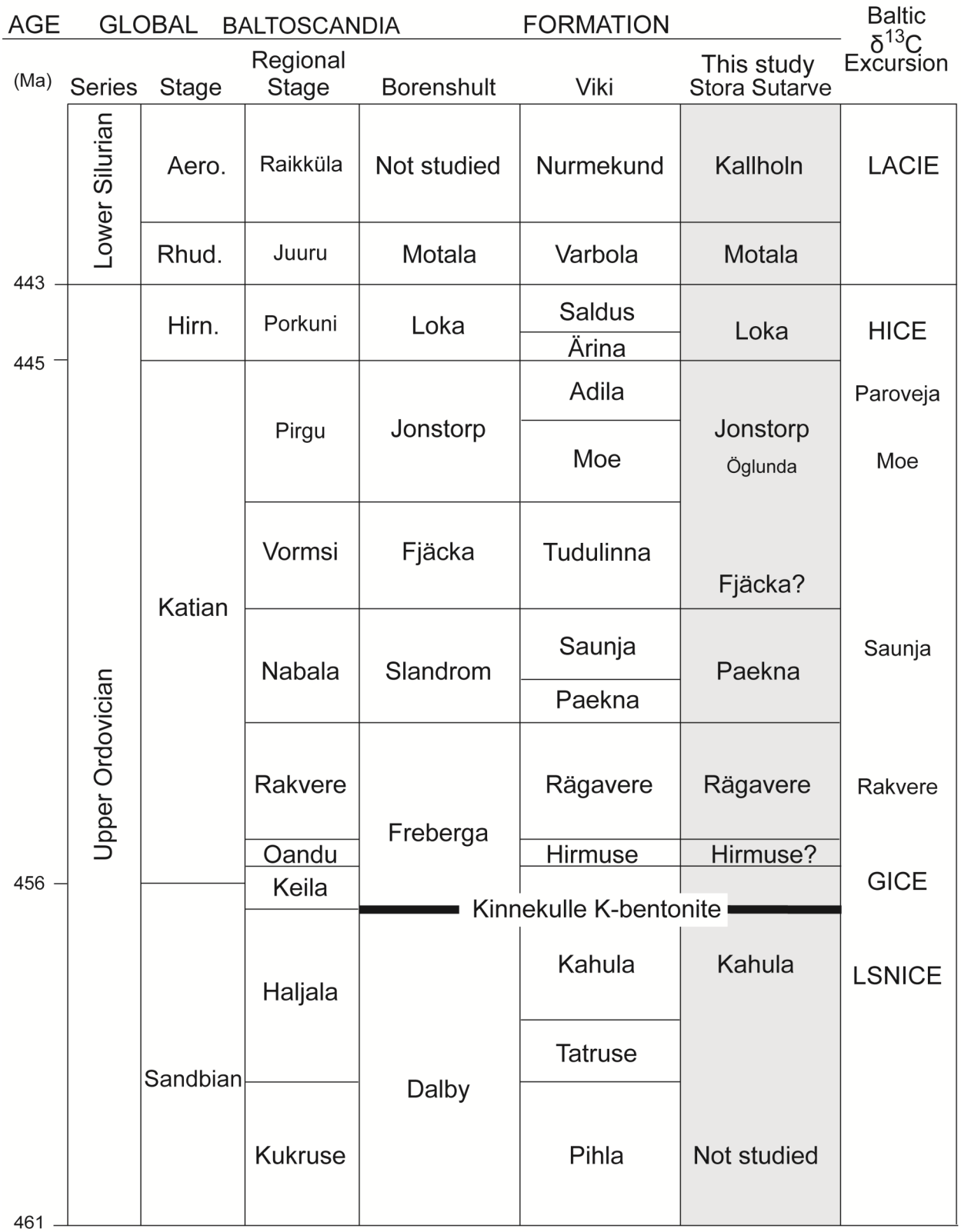


*Fig. 1.* Upper Ordovician stratigraphy of drill cores from the Baltoscandian basin correlated with the Baltic $\delta^{13}C$ excursions. The Borenshult formations are from Bergström et al. (2011). The Viki formations are from Põldvere (1998). The Baltic $\delta^{13}C$ excursions are from Ainsaar et al. (2010) and Bauert et al. (2014). The studied Stora Sutarve core is marked in grey.

Coquinas of Hindella and coquinas of Brevilamnulella have been identified within the Boda Limestone of the Hirnantian at several localities around Lake Siljan in central Sweden (Ebbestad et al., 2015; Kröger et al., 2015; Suzuki et al., 2009). The Hindella coquinas generally occur close to the peak of the HICE whereas the Brevilamnulella coquinas occur closely below the unconformity at the upper boundary of the formation (Ebbestad et al., 2015; Kröger et al., 2015; Suzuki et al., 2009). Similarly in Norway, abundant coquinas of Brevilamnulella kjerulfi were identified in the upper part of the Langøye Formation of Hirnantian age (P. Brenchley & Cocks, 1982; see also Calner et al. 2021).

The Hirnantian Stage in the East Baltic area (here named the Porkuni regional stage) varies in thickness from a few meters to ca 20 m. The stage constitutes the Kuldiga and Saldus formations in the Livonian Basin (extension of the Central Baltoscandian Confacies Belt) and the Ärina Formation in the North Estonian Confacies Belt (Harris et al., 2004; Jaanusson, 1995). In the Viki core from the Estonian island Saaremaa, the Hirnantian stage is 3.4 m thick and constitutes the Ärina and Saldus formations (Põldvere, 1998). The drill site is positioned in the marginal area of the North Estonian Confacies Belt (Jaanusson, 1995; Põldvere, 1998). The Ärina Formation is here developed as an argillaceous limestone (Põldvere, 1998). The lower Piltene member of the Saldus Formation is an oolitic limestone whereas the upper Broceni member is a quartz-rich, laminated and finely crystalline limestone (Põldvere, 1998). The δ13C values of the HICE in the Viki core show a rapid rise from baseline values around -1‰ in the Adila Formation to +2‰ in the Ärina Formation and reach its peak at +5.2‰ in the oolitic Piltene Member of the overlying Saldus Formation (O. Hints et al., 2014). The δ13C values then display a rapid drop to a plateau of +3‰ in the Broceni Member of the Saldus Formation, followed by a drop to baseline values between -1‰ to 0‰ (O. Hints et al., 2014).

As mentioned above, prominent jumps in the δ13C record, normally at the base and top of the anomaly imply stratigraphic hiatuses in the Hirnantian Stage (Brenchley et al., 2003). These two gaps are inferably related to non-deposition and/or erosion when sea-level fell due to the two ice-sheet advances associated with the Hirnantian Stage (Brenchley et al., 2003; Sutcliffe et al., 2000). The two hiatuses occur throughout localities in Europe, North America and China and was referred to as HA and HB respectively by Bergström (2006). Interglacial warm water limestone facies sometimes occur between the two hiatuses, such as the oolitic and coral bearing Skultorp Member of the Loka Formation (Bergström, Lehnert, et al., 2012; Stridsberg, 1975).

Four regressions and three transgressions have been identified in the Porkuni regional stage of the Upper Ordovician, which corresponds to the Hirnantian Stage, in the East Baltic area of the Baltoscandian Basin (Kiipli & Kiipli, 2020). The cycles have successively higher amplitude regressions and weaker transgressions, which might be due to adding of ice to the ice-sheet remaining on Gondwana (Kiipli & Kiipli, 2020). The Porkuni regional stage has its lower boundary corresponding to the lower boundary of the S. taugourdeuai chitinozoan biozone (Kiipli & Kiipli, 2020) and the same biozone is confined within the LOGC-3 of Ghienne et al. (2014). Four eustatic cycles were also identified in the Oslo area of the Baltoscandian Basin (Calner et al., 2021). Based on the dating of the Hirnantian Stage to 0.47Ma +/- 0.34 Ma (Ling et al., 2019), the four cycles in the latter area were interpreted as fourth order cyclicity (eccentricity) of ca 100ka superimposed on the LOGC-2 and LOGC-3 cycles (Calner et al., 2021).

### 1.4 This study

The aim with the present study is to make a stratigraphic assessment of the Upper Ordovician to lowermost Silurian successions of the recently recovered Stora Sutarve drillcore from southernmost Gotland (Fig. 2). From a palaeogeographic perspective this is within the same Central Baltoscandian Confacies Belt as the Borenshult core, which is ca 260 km to the northwest (Fig 2). The Viki core at the margin of the North Estonian Confacies Belt is located ca 270 km to the northeast (Fig 2). The Stora Sutarve core therefore provides an opportunity for comparison with two well studied cores. The Hirnantian of the nearby Grötlingbo drillcore has been studied with respect to biostratigraphy (Männik et al., 2015), but until now, no carbon isotope chemostratigraphic study of the Hirnantian has been undertaken from the Gotland area. This study presents the first integrated Upper Ordovician to lowermost Silurian stratigraphy and chemostratigraphy, with an especially detailed account of the microfacies and carbon isotope chemostratigraphy of the Hirnantian Stage. Comparison is made to the Borenshult and the Viki cores. This study also includes an interpretation of relative sea-level changes during the Hirnantian Stage with comparisons to the sea-level model of Kiipli & Kiipli (2020) and the Late Ordovician Glacial Cycles of Ghienne et al. (2014).

## 2 Geological setting

The Baltoscandian basin was an epicontinental sea that covered most of the Baltic Shield in the Ordovician. The regional changes in sedimentary facies of the Ordovician segment of the basin fill, early formed the basis for the establishment of broad facies belts (Fig. 2) that reflect bathymetry and depositional depths of the basin – the so called 'confacies belts' of Jaanusson (Jaanusson, 1973). Furthest to the west and closest to the Caledonian orogeny is the confacies belt with the deepest shale facies including the Oslo and the Scanian confacies belts. The Central Baltoscandian Confacies Belt, which covers large parts of Sweden and extends into the Livonian Basin, is dominated by marl and argillaceous limestone facies. Further to the east is the limestone dominated North Estonian Confacies Belt (Harris et al., 2004; Jaanusson, 1973). The boundaries of the confacies belt are spatially fluid across time (Jaanusson, 1995) and Gotland is in a 'transitional zone' (Harris et al., 2004).

## 3 Material and methods

The Stora Sutarve drillcore was drilled near Hamra on southernmost Gotland (coordinates Sweref 99 N 6320673 E 699981; Fig. 2) by the Geological Survey

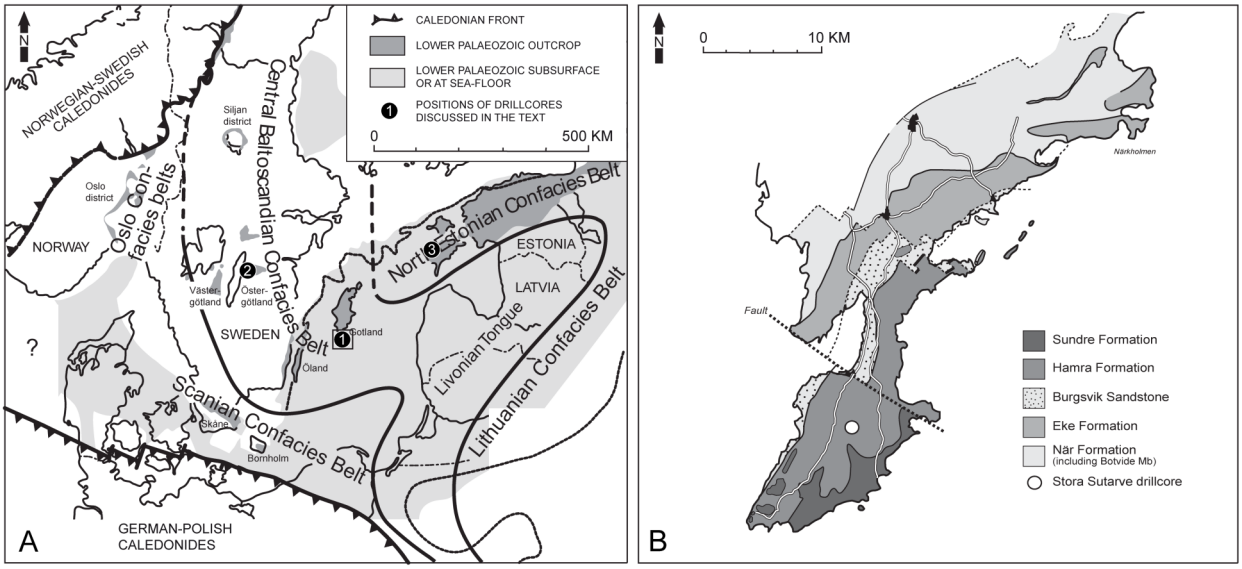


*Fig. 2.* A: Map of the Baltoscandian basin, with Confacies Belt, showing the location of coring of the (1) Stora Sutarve core, (2) the Borenshult core and (3) the Viki core. B: Map of the surface formations on the southern tip of the Island of Gotland with the coring location of the Stora Sutarve core marked. Modified from Calner et al. (2010).

of Sweden in 2018. Coring was stopped at -564.95 m in the Cambrian Faludden Sandstone and the core thus includes the entire Ordovician and most of the Silurian succession of the Baltoscandian Basin.

For the present study 34.5 m of the core from core boxes 81-86 were studied. This interval of the core was first photographed (Appendix A) and documented in terms of general lithology and stratigraphic changes. More than 40 pieces of the core, ranging from 10-35 cm in length, were subsequently split and polished. From these slabs, a total of 22 thin sections were produced at the Flügel Lab in Erlangen and provided by Oliver Lehnert. Polished slabs and thin sections were studied in a light microscope and a polarizing light microscope respectively, for overall analysis of microfacies textures.

A total of 391 whole-rock carbon isotope samples were collected from the core using a handheld micro-drill. Of the 391 samples, 189 samples were collected from the Loka Formation with the aim to sample as many carbonate microfacies as possible and make a high-resolution assessment of the HICE. Out of the 391 samples, 200 samples were collected from above and below the Loka Formation with roughly ten centimetres apart. A few samples were deliberately collected from the cement of spar-filled bioclasts and lithoclasts to evaluate the offset in $\delta^{13}C$. Carbonate powders were reacted with 100% phosphoric acid at 70°C using a Kiel IV carbonate device connected to a MAT 253 mass spectrometer. The $CO_2$ generated was used for analysing the carbon, calibrated by the Chinese national standard (GBW-04405) with a $\delta^{13}C$ value of 0.57 ± 0.03‰ (VPDB) during the analysis. The analytical precision is better than ±0.04‰ for $\delta^{13}C$. All the isotope analyses were carried out in the Stable Isotope Lab in the Nanjing Institute of Geology and Palaeontology, Chinese Academy of Sciences, China.

The Borenshult core, including thin sections (Bergström et al., 2011; Bergström, Lehnert, et al., 2012), was available in the core lab for direct comparison.

# 4 Stratigraphy and sedimentology of the Stora Sutarve core

The studied part of the core section constitutes mainly argillaceous, bioclastic limestone with subordinate mudstone and clean limestone (Fig. 3). A prominent feature is a series of 13 bentonites in the lower part of the studied interval. Based on the herein established carbon isotope stratigraphy and lithological comparison with the Borenshult (Bergström et al., 2011; Bergström, Lehnert, et al., 2012) and the Viki cores (Põldvere, 1998), this series of bentonites is provisionally named the Kinnekulle bentonite complex and the studied interval as a whole can be subdivided into eight formations representing the uppermost Sandbian through lowermost Silurian. Due to overall lithological similarities with the Viki core, Estonian formation names have been preferred for the lower parts of the studied section. In the upper part, beginning from the Jonstorp Formation, Swedish formation names have been used. This is elaborated in respective formation description.

## 4.1 Kahula Formation

The Kahula Formation (Fig. 4A) of the Haljala regional stage ranges from -23.78 m to -18.72 m (thus at least 4.51 m thick), in the studied core material. It is a greyish crinoid packstone-grainstone with subordinate, wavy sub-centimetre thick beds of marl. Skeletal fragments are mainly derived from crinoids, trilobites and bryozoans whereas brachiopods and ostracods are subordinate. The formation includes thirteen bentonites, in ascending order at; -23.78 with a thickness of 47 cm; -21.88 m with a thickness of 9 cm; -21.70 m with a thickness of 17 cm; -21.45 m with a thickness of 6 cm; -21.19 m with a thickness of 3 cm; -20.88 m with a thickness of 23 cm; -20.47 m with a thickness of 5 cm; -20.26 m with a thickness of 7 cm; -20.11 m with a thickness of 7 cm; -19.88 m with a thickness of 1 cm; -19.1 m with a thickness of 4 cm; -19.0 m with a thickness of 9 cm; and at -18.81 m with a thickness of

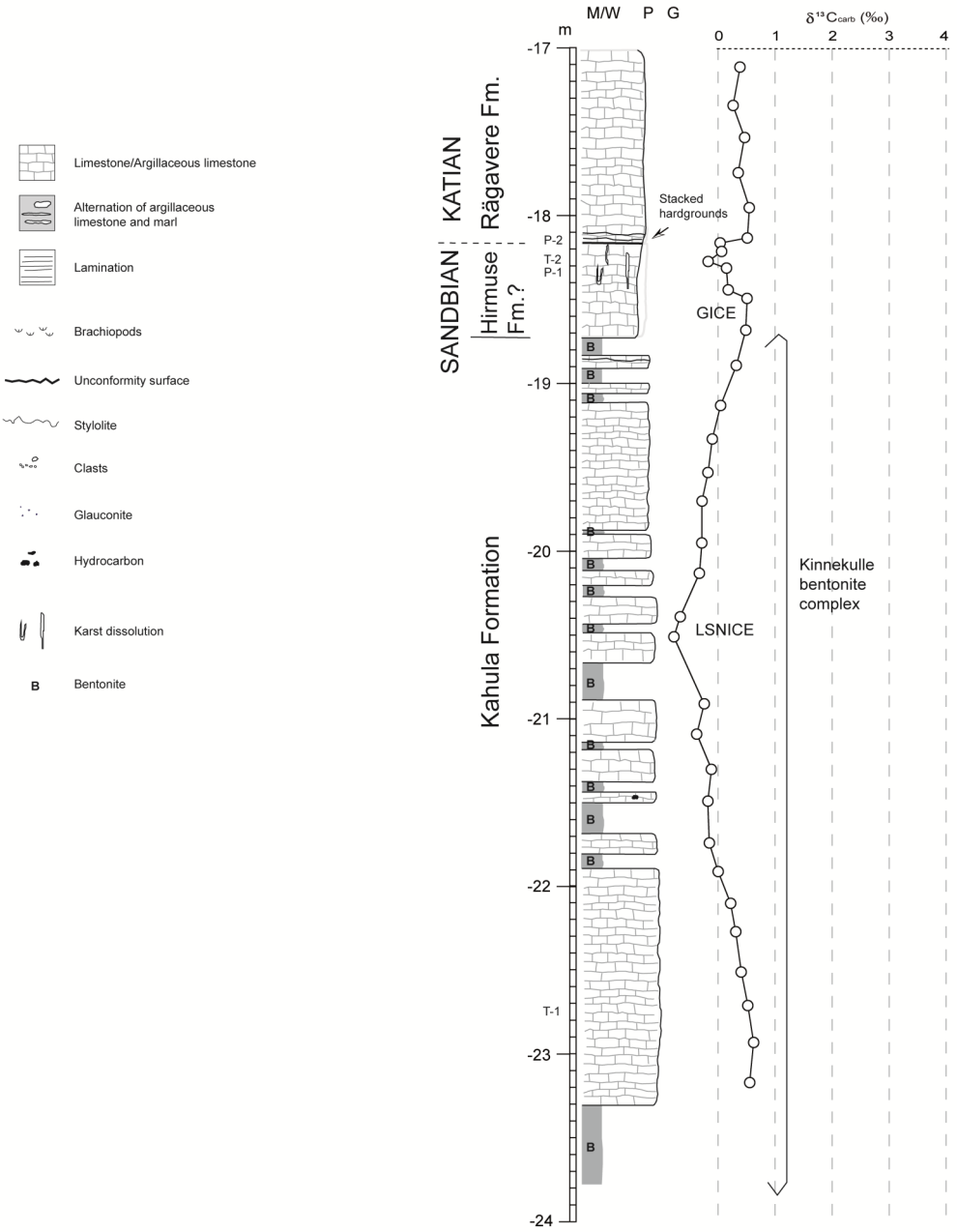


*Fig. 3.* Log of the stratigraphy of the Stora Sutarve core with $\delta^{13}C$ values plotted to the right. Identified excursions in the $\delta^{13}C$ plot includes LSNICE = Lower Sandbian Negative Isotope Carbon Excursion, GICE = Guttenberg Isotope Carbon Excursion, Moe excursion, HICE = Hirnantian Isotope Carbon Excursion and Late Aeoronian CIE = Late Aeoronian Carbon Isotope Excursion. In the top of the log is the Dunham classification for carbonate sedimentary rocks M/W = mudstone/wackestone, P = packstone, G = grainstone. To the left of the log T = thin section sample, P = polished slab, marks the stratigraphic position for microfacies study, illustrated herein.

7 cm. Microstylolites, small pyrite grains, blackened grains and fractures filled with black calcite occurs sparsely. There is a possible conglomerate bed between -22.12 m and -22.02 m. The conglomerate clasts are a grainstone, with similar skeletal fragments as within the enclosing formation. The conglomerate matrix is a mix of clay/marl, bioclasts and smaller reworked clasts. A cavity filled with hydrocarbons and large calcite crystals occurs at -21.49 m. Connected to the cavity are sub-millimetre thick fractures filled with black calcite. The lithology changes gradually upwards into a wackestone/packstone, with a pure carbonate matrix without detrital clay weathering products. One centimetre below the uppermost bentonite bed, at -18.81 m, is a mineralized hardground. The upper boundary of the formation is provisionally set at the top of the thirteenth and uppermost bentonite. This section of the core has been designated to the Kahula Formation due to overall lithological similarities to the Kahula Formation of the Viki core, which also includes multiple bentonite beds and a level with a conglomerate (Põldvere, 1998, p. 9). The lithology is different from the greenish limestone with wavy marl beds in the Dalby and Freberga formations of the

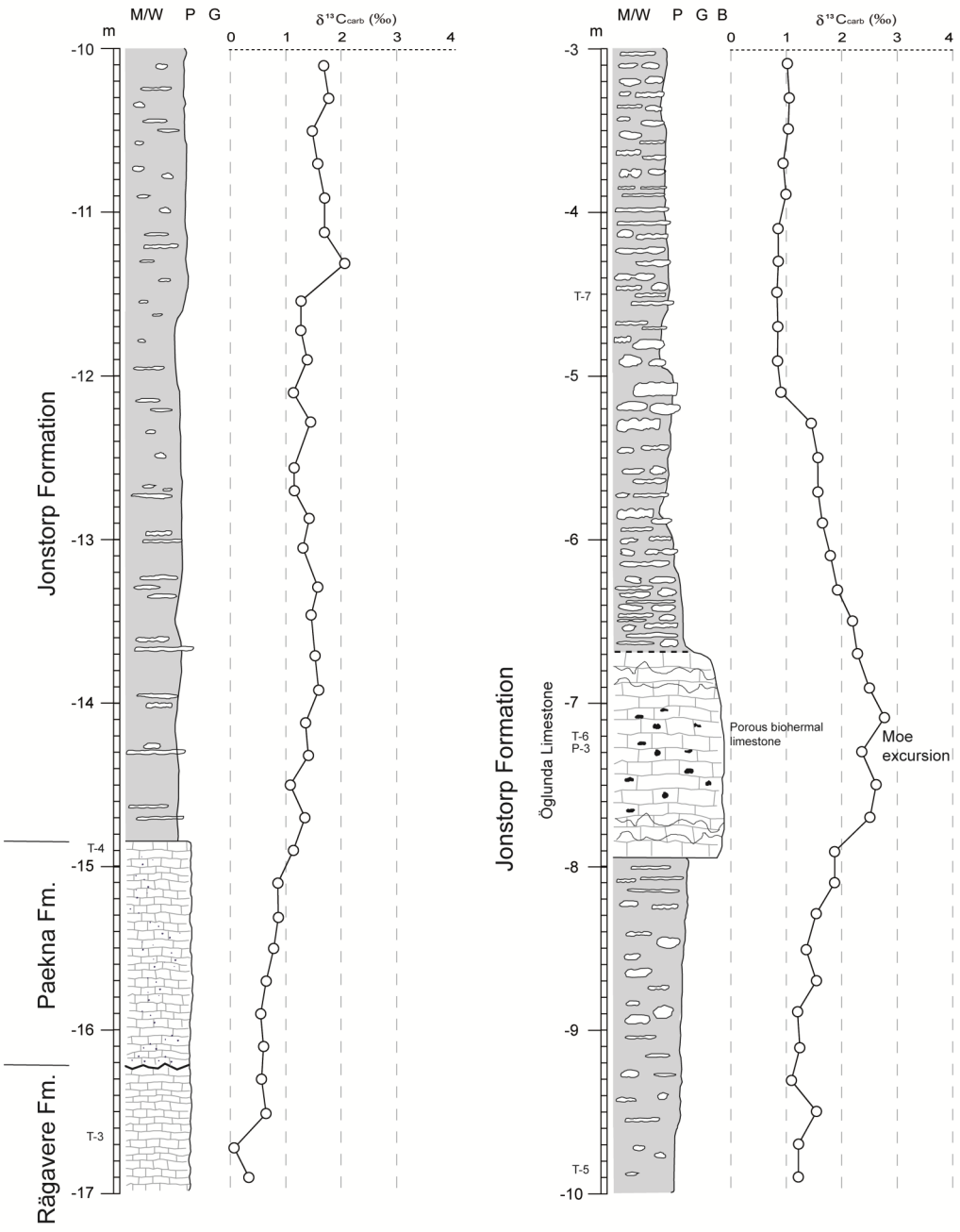


*Fig. 3.* Continued.

Borenshult core. No whole cystoids, which is characteristic of the Dalby Formation in the Borenshult core (Bergström et al., 2011), occurs in the studied interval of the Stora Sutarve core.

## 4.2 Hirmuse Formation

The base of the Hirmuse Formation (Figs. 4B and 5A) of the Oandu regional stage is set immediately above the uppermost bentonite bed of the bentonite complex and ranges from -18.72 m to -18.18 m (0.54 m thick). It is a light grey, dense wackestone; in places light greenish or bluish. Much of the matrix is interpreted as recrystallized carbonate from microbial activity. Skeletal fragments are mainly derived from crinoids, bryozoans, ostracods, trilobites and brachiopods whereas gastropods are subordinate. Bioturbation is sparse and includes burrows of the genus *Planolites*. Fractures ranging from millimetres to one centimetre in thickness and several centimetres long are common. The fractures are filled with large blocky calcite crystals that are sometimes dark in colour, inferably due to inclusions of hydrocarbons. Pyrite is abundant and ranges in size from minute grains to mottles of several millimetres. The upper boundary of the formation is set at the first of a series of stacked mineralized hardgrounds (Fig. 5B). The formation shows sign of possible freshwater diagenesis in the form of vertical fissures filled with coarse calcite spar. This lithology has been designated as the Hirmuse Formation as it is transitional between the inferred Kahula and Rägavere formations. The Hirmuse Formation corresponds roughly to Upper Freberga also known as Moldå Formation, which represents a shallowing depositional environment (Bergström et al., 2011), which in this

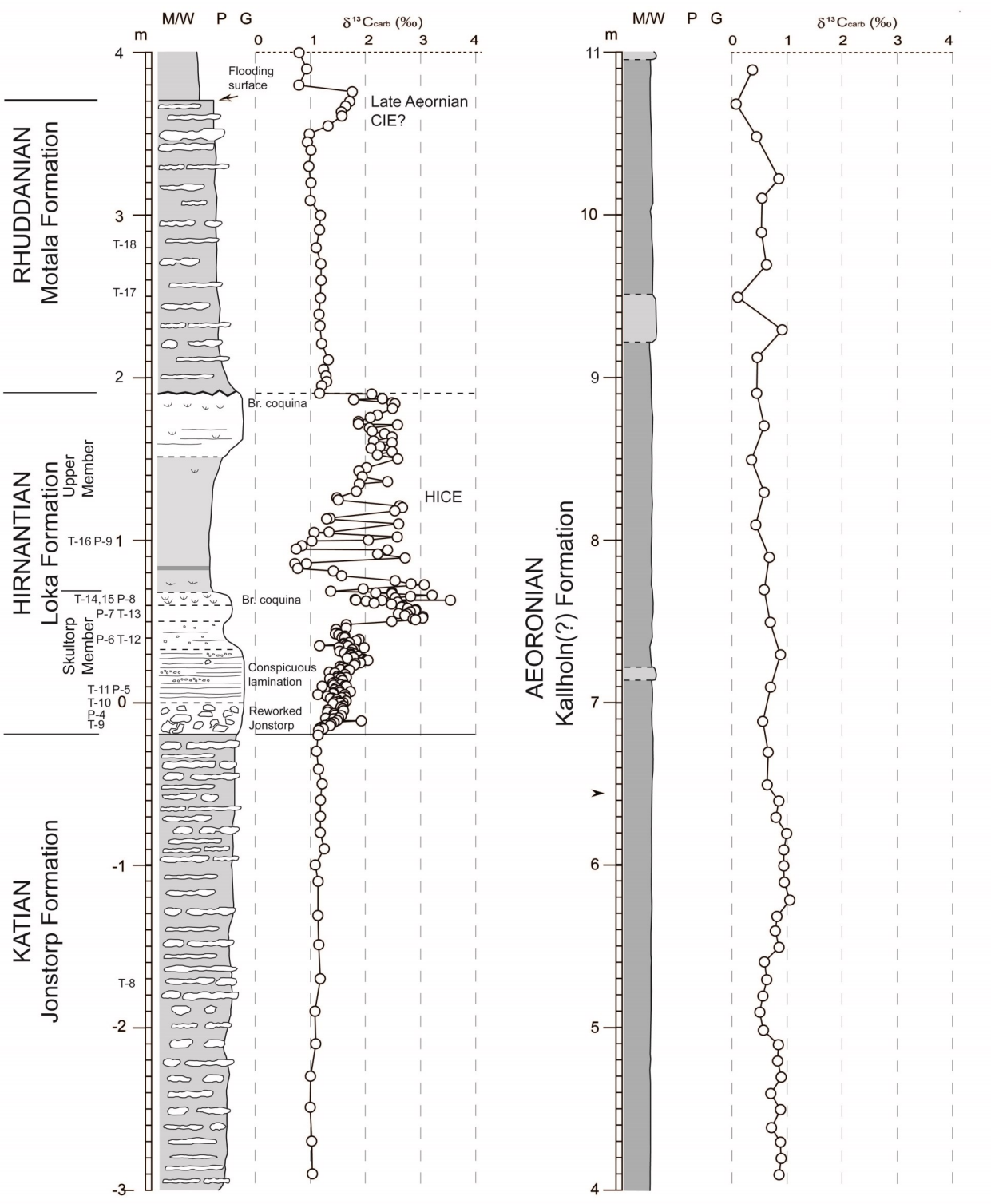


*Fig. 3.* Continued.

shallow part of the basin caused freshwater diagenesis. There is no lithology in the Borenshult core that is similar to the Hirmuse Formation of the Stora Sutarve core.

## 4.3 Rägavere Formation

The Rägavere Formation (Fig. 4C) of the Rakvere regional stage is separated from the underlying Hirmuse Formation by a phosphatized hardground (Fig. 5 B) and ranges from -18.18 m to -16.32 m (1.86 m thick). It is a light brownish grey packstone. Skeletal fragments are mainly derived from crinoids, trilobites, bryozoans, calcareous algae and ostracods whereas gastropods are subordinate. The calcareous algae belong to the genus *Vermiporella* and occur throughout the formation but are especially abundant between -17.80 m and -17.70 m. Sparse glauconite grains occur. Fractures of submillimetre-size are filled with calcite

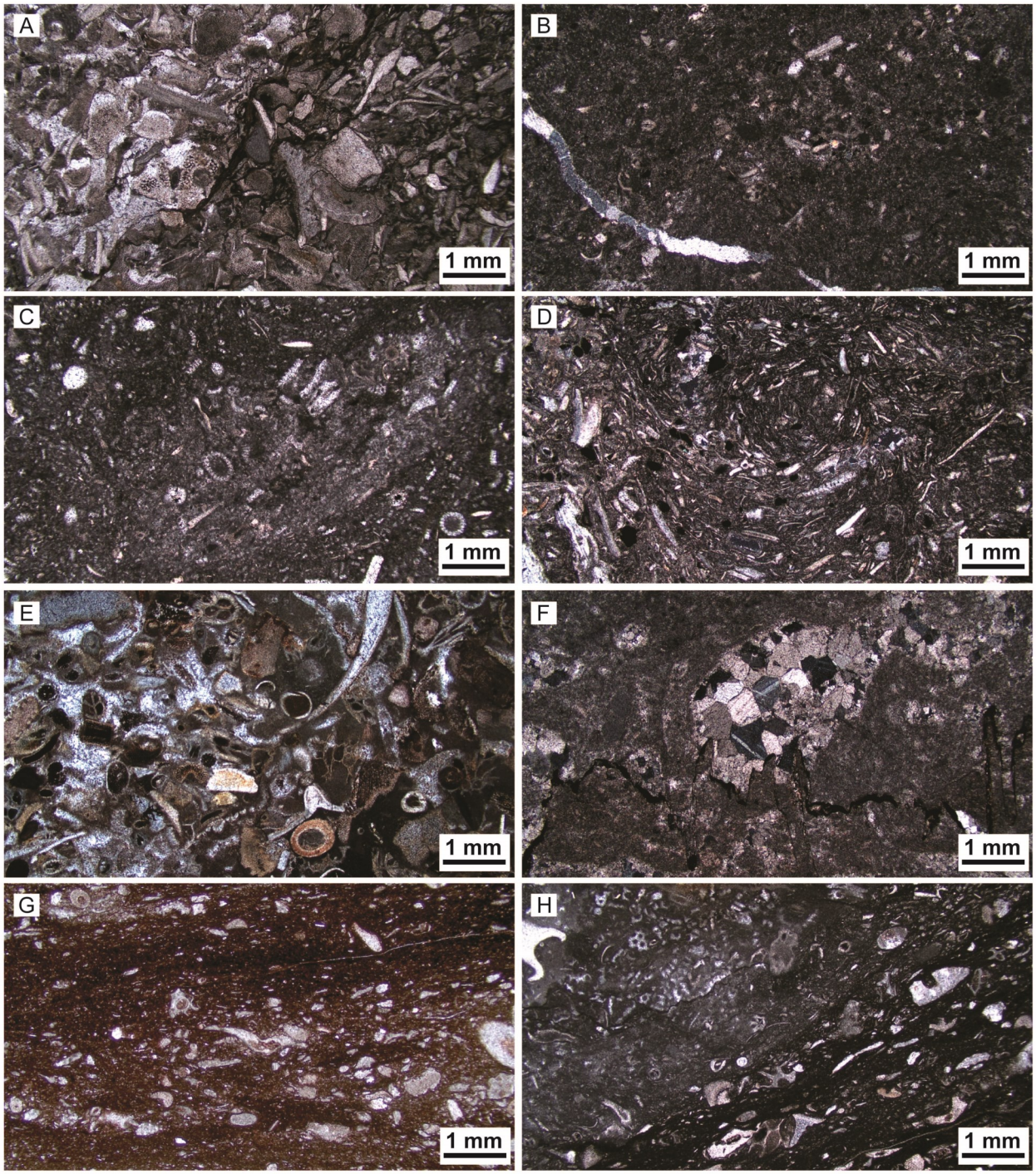


*Fig. 4.* Thin sections of the Upper Ordovician formations of the Stora Sutarve core. For the stratigraphic level of the thin section in parenthesis, see Fig. 3. A) Grainstone-packstone of the Kahula Formation with mainly crinoid fragments (T-1). B) Wackestone of the Hirmuse Formation (T-2). C) Packstone of the Rägavere Formation with calcareous algae and crinoid fragments (T -3). D) Strongly bioturbated packstone of the Paekna Formation with glauconite grains (black spheres) (T-4). E) Crinoid grainstone-packstone interval of the informal 'lower member' of the Jonstorp Formation (T-5). F) The Öglunda Limestone of the Jonstorp Formation with recrystallized calcareous algae (T-6). G) Reddish dense wackestone to packstone microfacies of the informal 'upper member' of the Jonstorp Formation with mainly crinoid fragments (T-7). H) Greenish bioclastic wackestone-packstone of the upper member of the Jonstorp Formation with crinoid fragments and calcareous algae (T-8).

which at some places is black in colour. At the base of the formation are stacked, amalgamated, phosphatized and partly pyritized hardgrounds which indicates episodic non-deposition. The upper boundary of the formation is set at a sharp change in the lithology, interpreted as an unconformity. At this unconformity is a cm sized coral. This unit has been designated as corresponding to the Rägavere Formation, based on the abundant presence of calcareous algae as well as on the lithological similarity with Vohma core from Estonia (Kröger et al., 2019; fig. 3b). The same similarities are seen in the Viki core (Põldvere, 1998; fig T-38 in

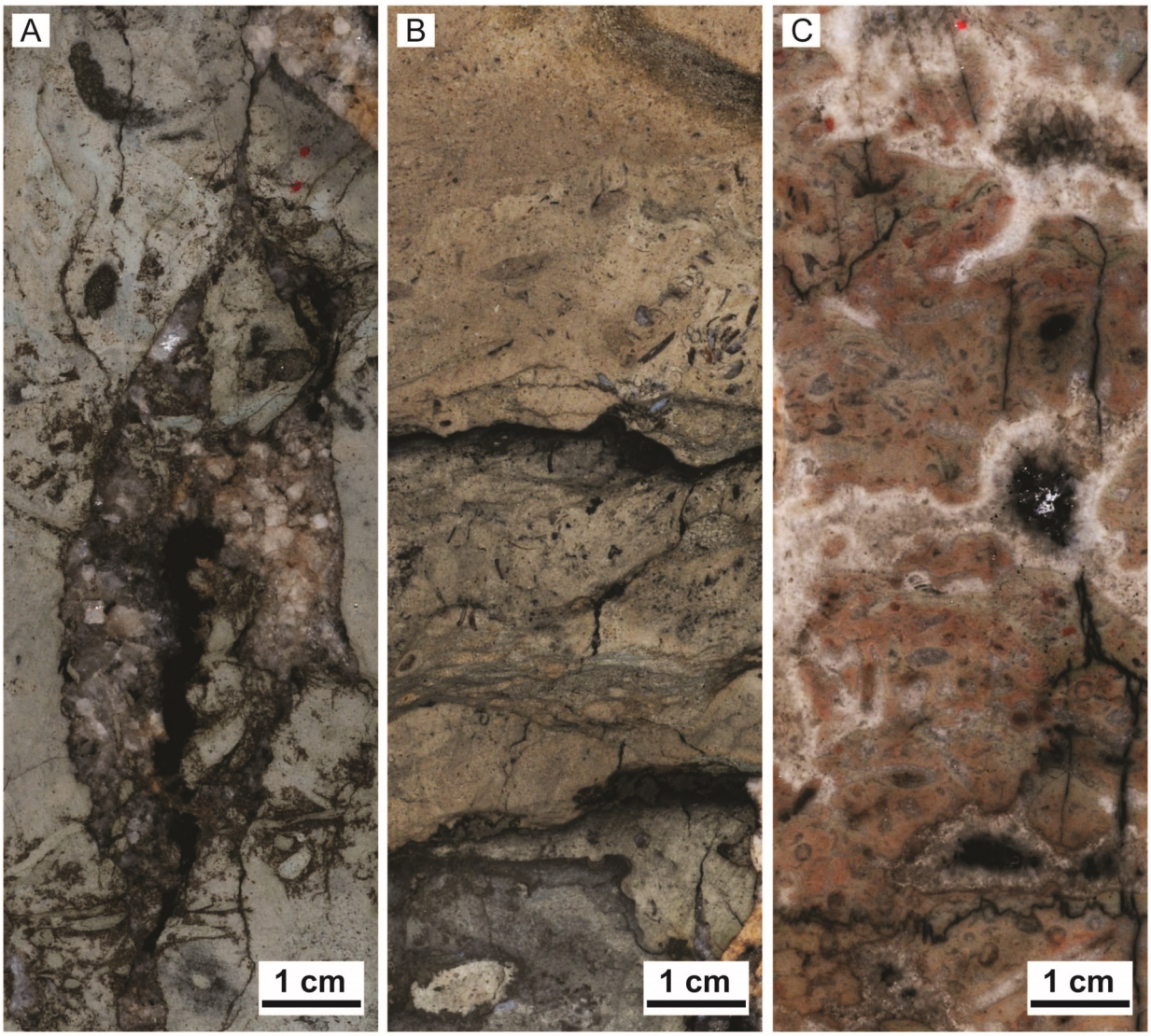


*Fig. 5.* Polished slabs of selected intervals from the core. For the stratigraphic level of the sample in parenthesis, see Fig. 3. A) The Hirmuse Formation (P-1) showing fissure with large blocky calcite crystals, blackened by hydrocarbons. B) The Hirmuse-Rägavere boundary (P-2), showing stacked mineralized hardgrounds. C) The Öglunda Limestone (P-3), showing a porous biohermal limestone (boundstone), mainly built up by recrystallized *in situ* calcareous algae of the genus *Dasyporella.* Contains

appendix 3). No similar lithology occurs in the Borenshult core, where no calcareous algae have been identified.

## 4.4 Paekna Formation

The Paekna Formation (Fig. 4D) of the Nabala regional stage is separated from the underlying Rägavere Formation by an unconformity. The formation ranges from -16.32 m to -14.81 m in the core (1.51 m thick). It is a light grey glauconitic packstone with submillimetre to millimetre thick wavy and horizontal beds of marl. Glauconite grains are very abundant throughout and distinctive for the formation. Skeletal fragments are mainly derived from crinoids, trilobites, brachiopods, bryozoans and ostracods. Stylolites and microstylolites are sparse. The upper boundary of the formation is not sharp, but transitional and marked by a rapid increase in marl/clay content and a synchronous rapid decrease in glauconite. This interval in the Stora Sutarve core shows a lithology similar to the Paekna Formation of the Viki core (Põldvere, 1998; fig. D-61 in appendix 2), especially in the high abundance of glauconite grains. There is no lithology in the Borenshult core that is similar to the Paekna Formation of the Stora Sutarve core.

It is notable that the Slandrom Formation, known from both the Borenshult core (Bergström et al., 2011) and the Viki core (as the Saunja Formation; (Põldvere, 1998)), is missing in the Stora Sutarve core. This formation belongs to the upper part of the Nabala regional stage and is normally easily identified due to it very fine-grained microcrystalline (aphanitic) texture (Calner et al., 2010). No sign of an unconformity or hiatus is present between the Paekna Formation and the overlying Jonstorp Formation.

## 4.5 Fjäcka shale

Across south and southcentral Sweden, a black shale known as the Fjäcka shale occurs at this stratigraphic level (Bergström et al., 2011, 2016; Calner et al.,

2010; Ebbestad et al., 2015). The Stora Sutarve core does not have this typical Fjäcka black shale, although a possible lateral mudrock equivalent occurs at this level in the core, see below.

## 4.6 Jonstorp Formation

The strata herein designated to the Jonstorp Formation have a tripartite subdivision in the informal 'lower member' and 'upper member' separated by the more calcareous Öglunda Limestone (cf. Bergström et al., 2011). Above Paekna, follows the lower member, which ranges from -14.81 m to -7.95 m in the core (6.86 m thick). In the basal portions of the Jonstorp Formation an argillaceous wackestone rich in crinoid debris (which is typical for the lower member of Jonstorp) is interbedded with a mudrock that inferably corresponds to and is the lateral facies expression of the Fjäcka Shale. This interfingering of two lithofacies extends for 2.31 m. From -12.5 m the lower Jonstorp lithology continues without the interbedded Fjäcka mudrock. The colour is mainly red but alternates to greyish green in some intervals. At -11.6 m, the lithology gradually changes to a marly crinoid packstone-wackestone. In some intervals from -9.6 m and above, the lithology changes to a crinoid packstone with inclusions of grainstone (Fig. 4E). These intervals have a rather atypical lithofacies for the Jonstorp Formation. Skeletal fragments are mainly derived from crinoids whereas bryozoans, trilobites, brachiopods, ostracods and gastropods are subordinate. At the upper boundary is a rapid decrease in clay along with the appearance of calcareous algae. There is no lower member equivalent in the Viki core as the Pirgu Stage starts with the Moe Formation (Põldvere, 1998, p. 10). The lower member of Jonstorp in the Borenshult core is similar to this lithology apart from the atypical intervals of crinoid packstone with grainstone inclusions. The lower member of Borenshult is greenish while Stora Sutarves lower member is mainly red.

The lower member of the Jonstorp Formation is overlain by the Öglunda Limestone (Figs. 4F and 5C), which ranges between -7.95 m to -6.7 m (1.25 m thick). This unit is a light grey and pinkish porous biohermal limestone (boundstone) with a wackestone matrix. The lithology is mostly built up of micro and millimetre-sized, recrystallized *in situ* calcareous algae of the genus *Dasyporella.* Centimetre-sized porosity occurs as several cavities filled with large calcite crystals and kerogen ranging mainly from about -7.74 to -7.0 m. There are also many vertical fractures filled with calcite and hydrocarbons. Skeletal fragments apart from the calcareous algae are subordinate and are mainly derived from trilobites and crinoids. Solution seams and stylolites occur abundantly throughout this unit. The upper boundary towards the upper member of the Jonstorp Formation is gradual, with an increase of micrite/clay and a decrease in the abundance of calcareous algae. This unit is lithologically similar to the Moe Formation of the Viki core (Põldvere, 1998; fig. D-53, D-54 and D-55 in appendix 2) and to the descriptions of the Moe Formation in L. Hints et al. (2005, pp. 232–234). The Öglunda Limestone has a similarly porous lithology as in the Borenshult core but with the addition of calcareous algae and hydrocarbons.

Strata referred to the upper informal member of the Jonstorp Formation ranges between -6.7 m to -0.19 m in the core (6.51 m thick). These constitute wavy beds of marl between nodules of limestone that is a crinoid packstone-wackestone and that varies between red (Fig. 4G) and greenish-grey (Fig. 4H) in colour. The skeletal fragments are mainly derived from crinoids, trilobites, bryozoans, brachiopods, calcareous algae and ostracods with subordinate gastropods. There are a few calcareous algae in the lowermost 0.25 m of the unit. The upper boundary marked by a rapid change to a reworked conglomeratic lithology of the lowermost Loka Formation. The Jonstorp Formation of Borenshult is similar to this lithology, except that the upper member is entirely red in that core whereas, the upper member in the Stora Sutarve core varies between greenish and red.

## 4.7 Loka Formation

The Loka Formation is generally a packstone to grainstone unit and ranges from -0.19 m to 1.9 m (2.09 m thick) in the core (Figs. 6 and 7). The formation includes a basal subunit with conglomeratic texture (Figs. 6A and 7A). The lithoclasts of this lower conglomerate have a similar microfacies, rich in calcareous algae, as the immediately underlying upper Jonstorp Formation. This implies that the Jonstorp-Loka contact is not fully conformable although no distinct erosional surface is obvious from the core section and the stable carbon isotope stratigraphy across the boundary does not support any substantial hiatus. The clasts of the basal unit are embedded in a bioclastic packstone-grainstone matrix, with a few rare ooids. From 0 m, the bioclastic packstone-grainstone is conspicuously laminated with very thin strings of organic-rich mudstone with fairly abundant silt-sized quartz (Figs. 6B and 7B-C). Lithoclasts of upper Jonstorp origin decrease upwards in size and number. A brachiopod coquina appears at 0.6 m (Figs. 6E and 7F-G) and at 0.68 m there is an abrupt change to a more clay-rich facies (Figs. 6 F and 7H). From around ~1.52 m there is a gradual change back to packstone-grainstone with wavy marly interbeds. This interval includes a second brachiopod coquina at 1.75 m. Skeletal fragments mainly derived from crinoids, trilobites, brachiopods, bivalves and ostracods with subordinate gastropods and rugose corals. The upper boundary of the Loka Formation is irregular with at least 1 dm relief and is a conspicuous unconformity. The Loka Formation in the core is overall similar to the argillaceous and oolitic limestones of both the Loka Formation in the Borenshult core and the Saldus Formation in the Viki core. For purpose of detail, the Loka Formation is herein further subdivided into seven lithological subunits in the petrography section below (Fig. 9).

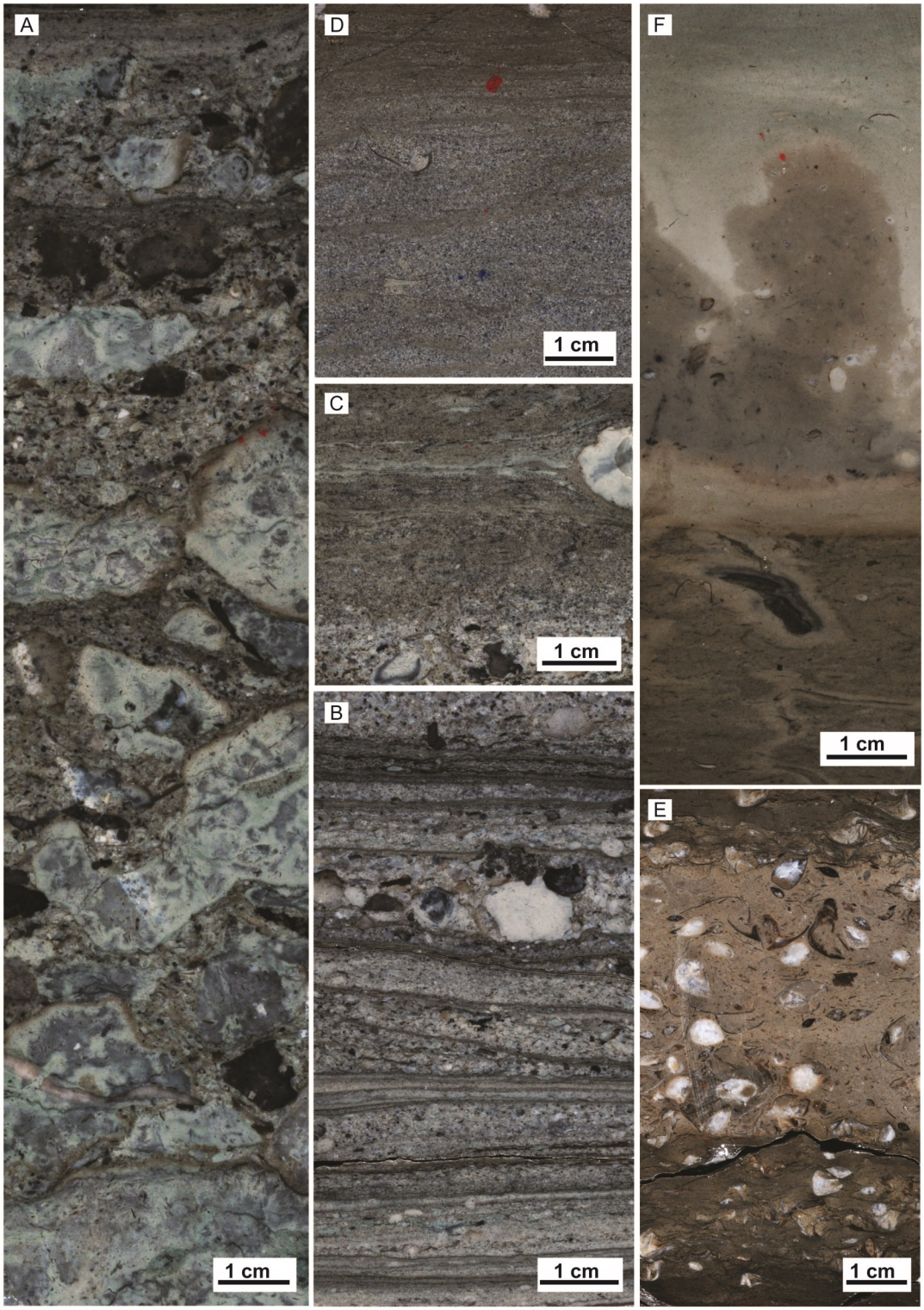


*Fig. 6*. Polished slabs showing the carbonate microfacies of the Loka Formation. For the subunit and stratigraphic level of the polished slab in parenthesis see Fig. 3. A) Section ranging from -0.17 m to 0.02 m (subunit A, P-4) showing abundant, light bluish-grey reworked clasts that in thin section display a microfacies dominated by calcareous algae and that is identical to the upper portions of the underlying Jonstorp Formation. The matrix between the clasts is a bioclastic packstone (lower part) or bioclastic grainstone with rare ooids (upper part). B) Section ranging from 0.02 m to 0.08 (subunit B, P-5) showing laminated grainstone-packstone sets separated by thin lamina of organic rich mudstone. C) Section ranging from 0.31 m to 0.355 m (subunits B-C, P-6) showing the boundary of subunit B to the overlying wackestone with streaks of organic-rich mud of subunit C. D) Section ranging from 0.52 m to 0.59 m (subunit D, P-7) showing a well-sorted quartz-rich packstone, almost approaching a calcareous siltstone, with streak of organic rich mud. E) Section ranging from 0.595 m to 0.675 m (subunit E, P-8) showing a distinct brachiopod coquina. The more calcareous middle part contains several whole, articulated and spar-filled brachiopods. The more mud-rich lower and upper parts contain brachiopod fragment with a preferred horizontal orientation. F) Section ranging from 0.955 m to 1.065 m (subunit F, P-9) showing a fine-grained wackestone with a calcareous rich matrix.

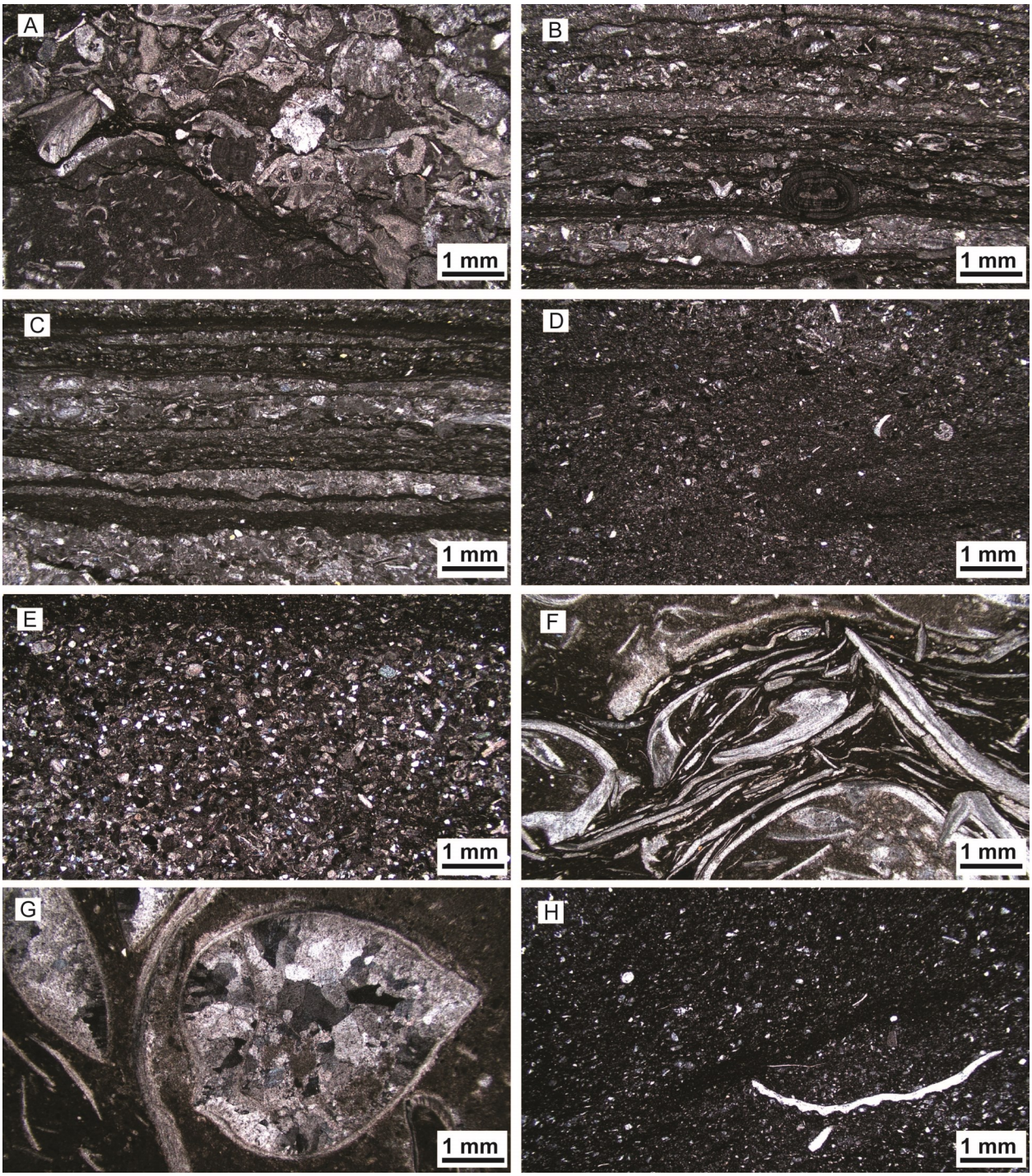


*Fig. 7.* Thin sections of the Loka Formation in the Stora Sutarve core. For the subunit and stratigraphic level of the thin section in parenthesis see Fig. 3. A) From ca -0.13 m (subunit A, T-9). Reworked clasts (lower left) with similar calcareous algae wackestone microfacies as the Upper Jonstorp in a grainstone-packstone matrix with mainly crinoid and bryozoan fragments. B) From ca 0 m (subunit B, T-10). Laminated grainstone-packstone sets separated by thin lamina of organic-rich mudstone. Mainly crinoid fragments are seen in the grainstone-packstone sets of this thin section. A concentric laminated ooid with a crinoidal core is seen in the lower middle part of the photograph. C) From ca 0.08 m (subunit B, T-11). Detail of laminated grainstone-packstone sets separated by organic-rich mud. Mainly crinoid fragments are seen in the grainstone-packstone sets of this thin section. D) From ca 0.40 m (subunit C, T-12). Fine-grained bioclastic wackestone-packstone with crinoid and bryozoan fragments. E) From ca 0.58 m (subunit D, T-13) A well-sorted quartz-rich packstone, almost approaching a calcareous siltstone. Apart from quartz grains, crinoid fragments are also seen in this thin section. F) From ca 0.67 m (subunit E, T-14) brachiopod fragments with preferred orientation from the brachiopod coquina. G) From ca 0.65 m (subunit E, T-15). Whole articulated and spar-filled brachiopods from the brachiopod coquina. The larger brachiopod has been identified as *Brevilamnulella.* H) From ca 1.05 m (subunit F, T-16). Fine-grained bioclastic wackestone with a strophomenoid brachiopod.

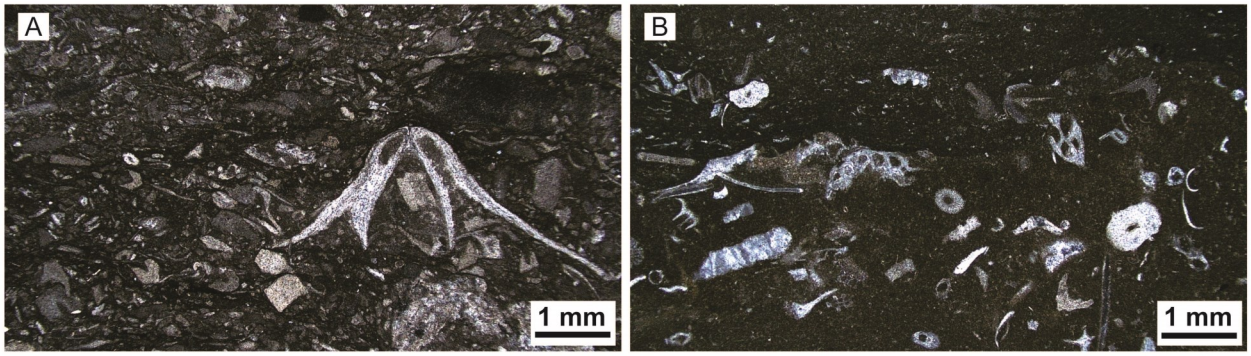


*Fig. 8.* Thin sections of the Motala Formation. The stratigraphic level of the thin section in parenthesis, see Fig. 3. A) Crinoidal packstone from ca 2.54 m (T-17). Mainly crinoid fragments and a relatively larger brachiopod fragment are seen in this thin section. B) Bioclastic wackestone from ca 2.83 m (T-18). Mainly crinoid and bryozoan fragments are seen in this thin section.

### 4.8 Motala Formation

The strata above the upper unconform boundary of the Loka Formation is herein provisionally assigned to the Motala Formation of Silurian Age (Fig 8). The formation ranges from 1.90 m to 3.71 m (1.81 m thick). It is a grey marly wackestone with nodular interbeds of reddish packstone. Skeletal fragments are mainly derived from crinoids, ostracods, brachiopods, trilobites whereas gastropods are subordinate. The upper boundary of the formation is associated with a sharp change to a siliciclastic mudstone at 3.7 m, this is interpreted as a flooding surface. The lithology is similar to that of the informal middle member of the Motala Formation in the Borenshult core, which is a greenish grey wackestone with nodules of reddish wackestone (Bergström et al., 2011). Thus the Stora Sutarve core might be missing the informal lower and upper members of this formation as seen in the Borenshult core. In the Viki core, the Varbola Formation of the Juuru regional stage, above the Porkuni regional stage, display less similarities as it is described as a cryptocrystalline limestone with patches and interbeds with marlstone and argillaceous limestone. It contains glauconite and pyritized discontinuity surfaces (Põldvere, 1998).

### 4.9 Kallholn Formation

The black mudstone above the Motala Formation is herein provisionally referred to as the Kallholn Formation (Bergström, Eriksson, et al., 2012). It is separated from the underlying Motala Formation by a sharp boundary and ranges from 3.71 m to at least 11.09 m (minimum 7.38 m thick), which is at the end of the studied core material. The formation constitutes a grey mudstone with centimetre sized mottles of pyrite, sometimes with sub-centimetre close to euhedral pyrite crystals. Macro fossils are dominated by graptolites and bivalves. Throughout the mudstone are a few 5-20 cm thick interbeds of bioturbated grey wackestone with a higher calcareous content in the matrix. Skeletal fragments in the wackestone intervals are mainly derived from brachiopods, crinoids and trilobites. The Viki core does not have a mudrock interval above the Hirnantian. The Borenshult core ends before any appearance of mudrock.

## 5 Petrography of the Loka Formation

### 5.1 Lithological subunits and microfacies

Based on lithological variation the Loka Formation (ranging from -0.19 m to ~1.90 m) can be divided into seven lithological subunits, A to G (Fig. 9).

The lowermost subunit A ranges from -0.19 m to 0 m (Figs. 6A and 7A). The unit has a conglomeratic texture with slightly rounded clasts that are ca 0.5 cm to 2 cm in diameter. The lithoclasts are light grey and have a similar microfacies as the upper Jonstorp Formation, containing the same distinct calcareous algae. A few of the lithoclasts are dark through mineralization. In the lowermost part between -0.19 m and -0.16 m, the matrix between the clasts is composed of the typical greenish Jonstorp marl. From -0.16 m to 0 m the matrix changes to a packstone-grainstone microfacies typical of the overlying subunit B. This packstone-grainstone matrix includes rare ooids. The ooids are dark in colour and occur with radial symmetry, concentric symmetry and radial-concentric symmetry. Most have a spherical shape but a few are elongated and some are fragmented. The majority of ooids have a crinoid bioclast as nucleus. Skeletal fragments are mainly derived from crinoids whereas bryozoans, trilobites, brachiopods, ostracods and calcitarchs are subordinate.

Subunit B ranges from 0 m to 0.32 m (Figs. 6B and 7B-C). It is conspicuously laminated and is lacking any larger conglomeratic clasts. It is composed of a few millimetre thick sets of packstone-grainstone, each separated by thin laminae of quartz and organic-rich mudstone with scattered bioclasts or microscopic bioclastic lenses. The quartz grains are mainly in the silt fraction. The lithoclasts, with a similar microfacies as upper Jonstorp, continues upward in this unit but with a decrease in both size and numbers. Ooids still occur in this subunit. Skeletal fragments are mainly derived from crinoids whereas bryozoans, trilobites, brachiopods, ostracods and calcitarchs are subordinate.

Subunit C ranges from 0.33 m to 0.505 m (Figs. 6C and 7D). It is a wackestone-packstone. The lamination is much less distinct and is replaced by streaks of clay. At 0.38 m is the last identifiable lithoclast of upper Jonstorp origin. Skeletal fragments are much fewer

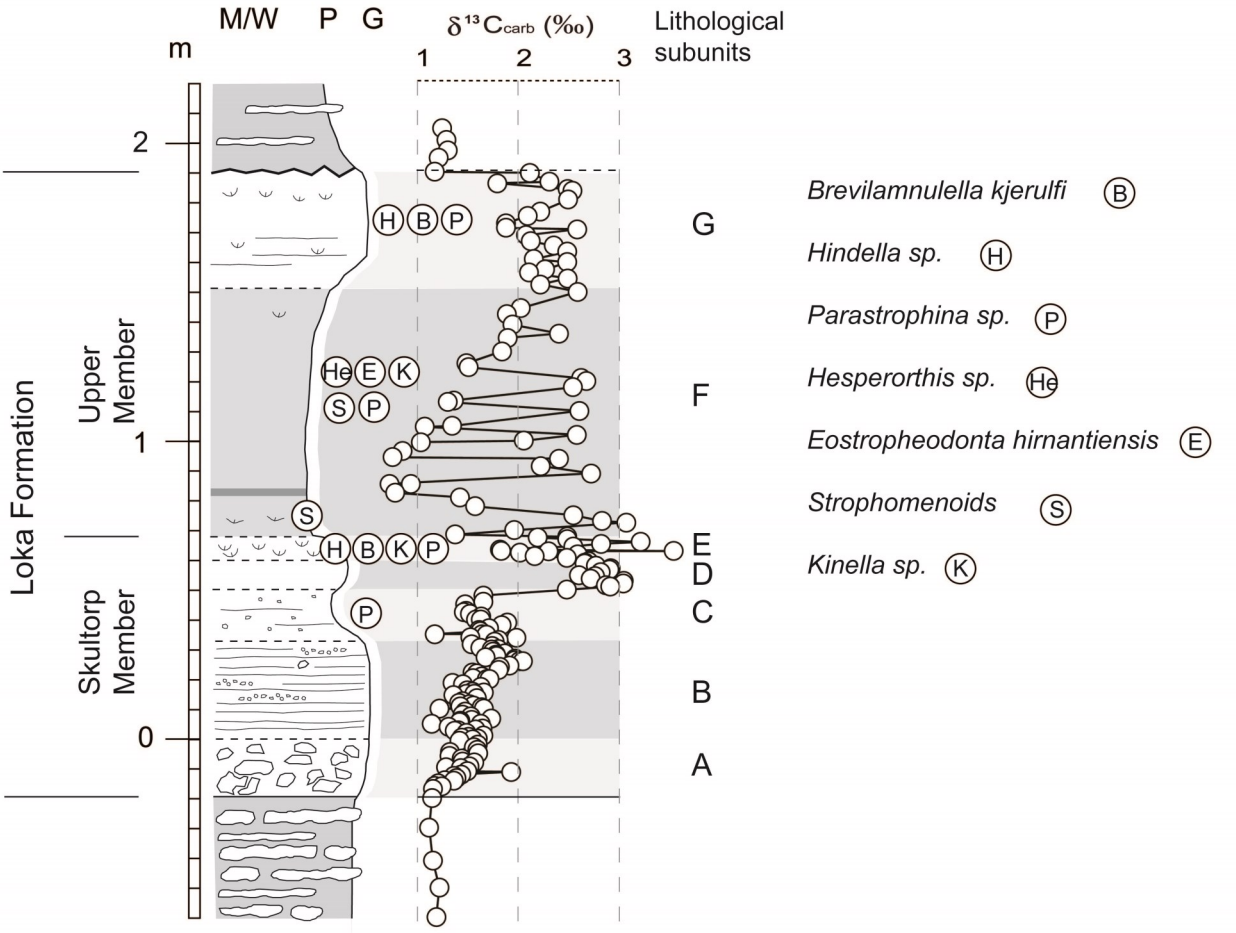


*Fig. 9.* Detailed lithological stratigraphy (subunits A-G) together with a high-resolution plot of the HICE in the Loka Formation. The stratigraphic positions of identified brachiopods are marked in the log.

in abundance. Rare ooids still occurs in this subunit. Quartz grains are sparse. Skeletal fragments are mainly derived from crinoids whereas bryozoans, trilobites, brachiopods, calcitarchs and ostracods are subordinate. From 0.38 m and upward the skeletal fragments are much fewer in numbers.

Subunit D differs from C by an increased content of quartz grains and skeletal fragments and it ranges from 0.505 m to 0.60 m (Figs. 6D and 7E). It is a well-sorted quartz-rich packstone with streaks of organic-rich clay, almost approaching a calcareous siltstone. Rare ooids still occur. Skeletal fragments are mainly derived from crinoids whereas brachiopods, bryozoans, calcitarchs and trilobites are subordinate.

Subunit E ranges from 0.60 m to 0.68 m and is a brachiopod coquina packstone (Figs. 6E and 7F-G). The coquina is made up of whole, articulated brachiopods and brachiopod skeletal fragments. The matrix is darker and inferably organic-rich mud in the lowermost two centimetres and in the top 1.5 centimetres, whereas the middle part is more calcareous. The lower and upper parts contain disarticulated brachiopod shells orientated with their long axis parallel to the bedding whereas the middle part constitutes articulated spar-filled brachiopods without preferred sorting or orientation. Quartz grains are abundant in the top two centimetres but occur sparsely throughout the coquina.

Subunit F is separated from E by a rapid change to a more clay-rich facies and it ranges from 0.68 m to ~1.52 m (Figs. 6F and 7H). It is a brownish grey wackestone with sparse quartz grains. The most condensed dark mudrock of the entire Loka Formation is situated between 0.81 m and 0.82 m. Above there is a gradual upward increase in carbonate content. Skeletal fragments are few in numbers and are derived from brachiopods, crinoids, bryozoans, trilobites and gastropods (*Hormotoma*).

Subunit G is separated from F by a gradual change to packstone and the unit ranges from ~1.52 m to 1.90 m. It is a grey packstone-grainstone with wavy interbeding of greenish marl/clay. A second brachiopod coquina appears between 1.75 m to 1.82 m. Skeletal fragments are mainly derived from brachiopods, crinoids, trilobites, bryozoans and gastropods. The upper formation boundary of this subunit corresponds to the unconformity at the top of the Loka Formation.

## 5.2 Loka Formation biostratigraphy - A preliminary study of the brachiopod fauna

Identified brachiopods are marked in Figure 9. In the wackestone, above the lamination, in the upper part of subunit C *Parastrophina sp.* is identified at 0.43 m. In subunit E, *Brevilamnulella kjerulfi* (Fig. 7G) and *Hin-*

*della cassidea/ incidens* have both been identified in the brachiopod coquina along with *Kinnella* and *Parastrophina sp*. In subunit F, representing a more fine-grained, clay-rich facies, several strophomenoids have been identified between 0.68 to 0.80 m and around 1.26 m. Around 1.30 m *Parastrophina sp., Hesperorthis? sp., Kinnella? sp.* and *Eostropheodonta? Hirnantiensis* occur. In subunit G, *Hindella sp., Brevilamnulella kjerulfi* and *Parastrophina sp.* occur up to the unconformity and with greater abundance within the brachiopod coquina between 1.75 and 1.82 m. Out of the identified brachiopods, *Hindella, Kinella* and *Eostropheodonta* belong to the *Hirnantia* fauna whereas *Brevilamnulella, Parastrophina* and *Hesperorthis* belong to the Edgewood-Cathay fauna. If the subdivision of transitional benthic faunas is applied *Kinella* is associated with TBF-1, *Hindella, Parastrophina and Eostropheodonta* are associated with TBF-2 and *Brevilamnulella,* and *Hesperorthis* are associated with TBF-3 (Wang et al., 2019).

# 6 Upper Ordovician carbon isotope chemostratigraphy

## 6.1 Pre-HICE

Within the Kahula Formation (-23.23 m to -18.72 m) 21 $\delta^{13}C$ samples were analysed (Fig. 3). From -22.92 m with a value of 0.62‰, the $\delta^{13}C$ values decline slowly to a minimum of -0.78‰ at -20.50 m. A slow increase commences and the last value in the formation, just before the uppermost bentonite bed, shows a value of 0.32‰ at -18.88 m. Within the Hirmuse Formation (-18.72 m to -18.18 m) six $\delta^{13}C$ samples were analysed. Up to -18.48 m (0.51‰) the values continue the increasing trend from the Kahula Formation. A step-wise negative shift follows, with a drop to minimum -0.17‰ at -18.26 m. Within the Rägavere Formation (-18.18 m to -16.32 m) ten $\delta^{13}C$ samples were analysed. Values increase to and stabilize at a baseline of around ~0.30‰. At -16.72 m one value shows a negative shift to 0.07‰ directly followed by an increase to 0.65‰. Within the Paekna Formation (-16.32 m to -14.81 m) eight $\delta^{13}C$ samples were analysed. Values increase from 0.57‰ at -16.30 m to 1.14‰ at -14.90 m at the top of the formation. Within the Jonstorp Formation (-14.81 m to -7.95 m) 78 $\delta^{13}C$ samples were analysed, out of which 34 samples were from the lower member. Values are seen to fluctuate at a new increased baseline around 1.20‰ – 1.50‰. A temporary increase in one value to 2.07‰ is seen at -11.31 m followed by slightly higher baseline values that increase again just below the Öglunda Limestone. From the Öglunda Limestone, seven of the 78 Jonstorp samples were analysed. The slightly higher and increasing baseline continues to increase rapidly in the Öglunda Limestone and an excursion is evident. This excursion reaches a maximum of 2.77‰ at -7.09 m. From the upper member, 37 of the 78 Jonstorp $\delta^{13}C$ samples were analysed. A decrease from the excursion in the Öglunda Limestone continues from a value of 2.19‰ at -6.5 m and stabilizes at 0.91‰ at -5.1 m. A baseline around ~1.00‰ continues throughout the member to the upper boundary of the Jonstorp Formation.

## 6.2 HICE

For the purpose of detail, all $\delta^{13}C$ sample positions within the Loka Formation are plotted on the scanned core section as shown in Appendix B. The figure displays the details of the core and the variation in carbonate microfacies.

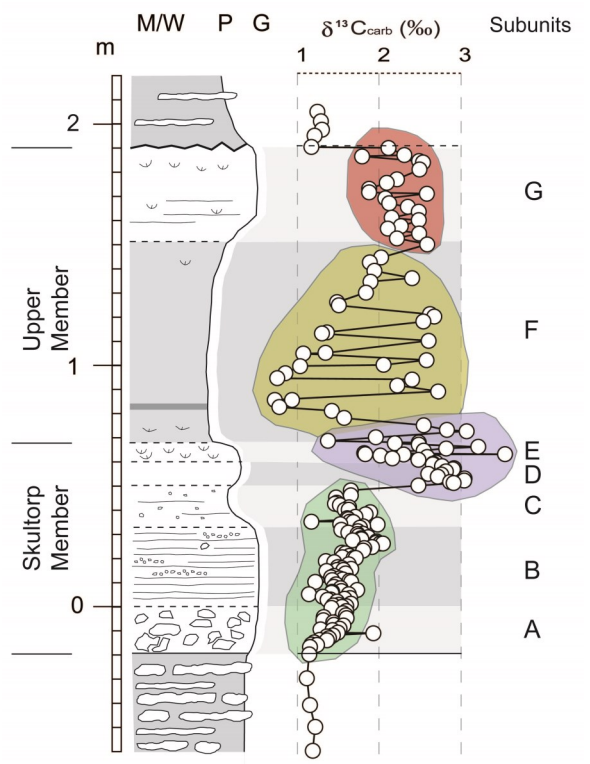


*Fig. 10.* The stratigraphy of the Loka Formation with the HICE plotted to the right. Four clusters of $\delta^{13}C$ values, with four respective different trends, are marked in colours. In green is a cluster of $\delta^{13}C$ values with an increasing trend in the rising limb. In blue is a cluster of peak $\delta^{13}C$ values. In yellow is a cluster of strongly fluctuating $\delta^{13}C$ values in the plateau interval. In red is a cluster of $\delta^{13}C$ values in the plateau with less fluctuation.

Within the Loka formation (-0.19 m to 1.9 m) and including the entire preserved HICE interval, 189 $\delta^{13}C$ samples were analysed (Figs. 3 and 10). The five topmost $\delta^{13}C$ values of the Jonstorp Formation have a mean of 1.16‰. From the base of subunit A is a steady increasing trend, which continues up to 1.54‰ at 0.221 m in subunit B. Sample BSU-109 at -0.112 m shows a positive deviation with a value of 1.92‰. This sample was taken from a dark, mineralized lithoclast with similar microfacies as upper Jonstorp and thus is reworked. From 0.221 m to 0.259 m, there is a jump up to 2.04 ‰. A slightly negative trend continues to 1.65‰ at 0.48 m. This negative trend is within subunits B and C. Sample SU-55 at 0.35 m shows a negative deviation with a value of 1.17‰. This sample was also taken from a reworked lithoclast with similar microfacies as upper Jonstorp. A particularly large jump follows to 2.48‰ at 0.5 m, still within subunit C. The next value is at 2.91‰ at 0.51 m in subunit D. A cluster of samples with high values, and with an average of 2.59‰, occurs between 0.51 m – 0.73 m. This cluster

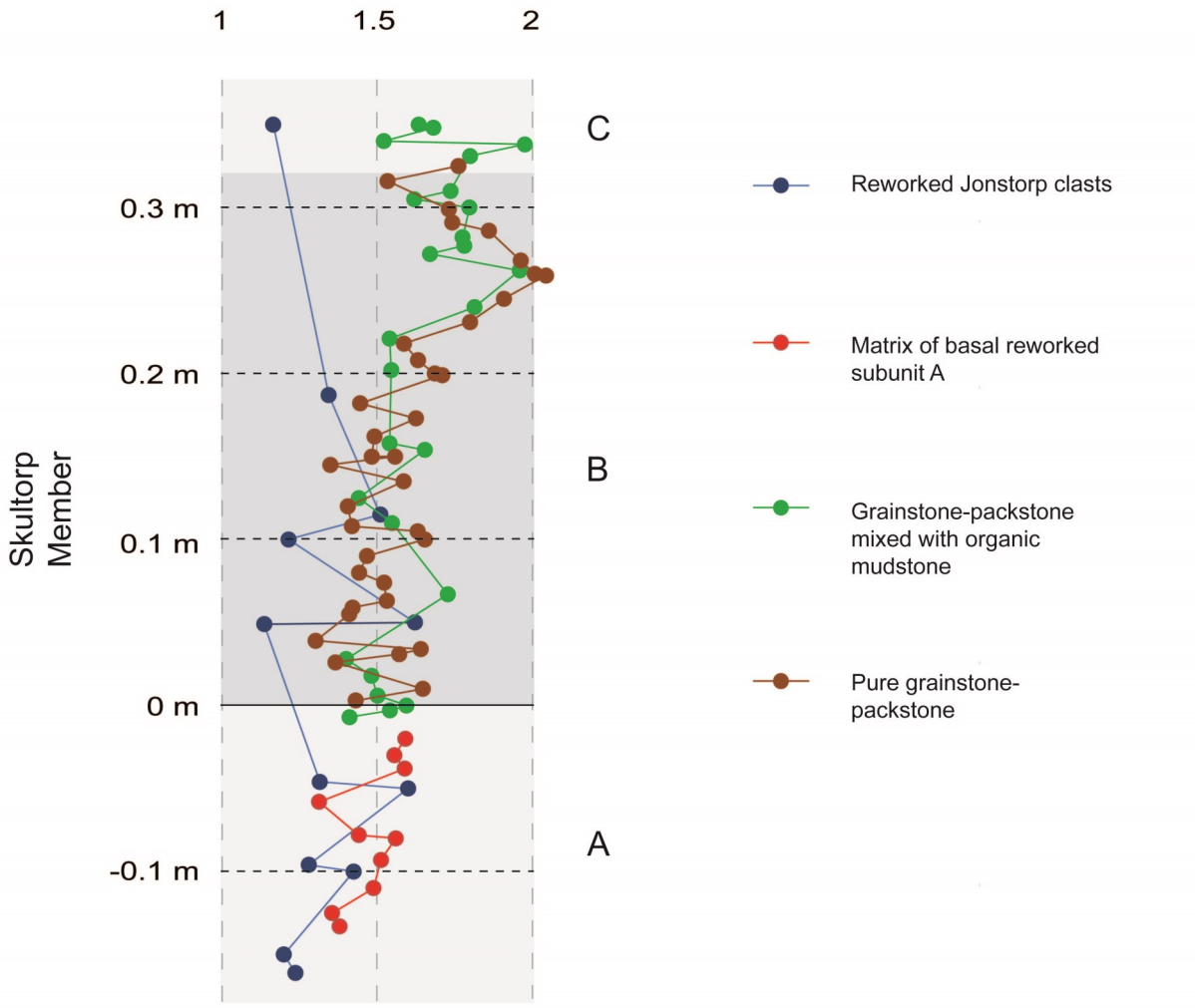


*Fig. 11.* High-resolution expression of the carbon isotope data during the first 0.5 m of the HICE. Note the slightly lower $\delta^{13}C$ values of the microfacies of reworked Jonstorp clasts (in blue).

is within subunit D, subunit E (the coquina) and at the lowermost part of subunit F. Subunit E shows relatively large fluctuation in the $\delta^{13}C$ values. A minimum value of 1.83‰ at 0.63 m was sampled from the calcite filling of an articulated brachiopod to highlight the offset caused by diagenesis. It is likely that some of the fluctuation in subunit E is caused by un-noticed spar-filled whole fossils of a finer size fraction and thus difficult to avoid when sampling. The maximum value of 3.54‰, also at 0.63 m, in subunit E (the coquina) marks the peak value in the Loka Formation and of the HICE in the Stora Sutarve core. Subunit F differs from all other subunits in having the most pronounced fluctuation in $\delta^{13}C$ values. It has an average value of ~1.80‰ with a minimum value of 0.72‰ at 0.855 m and a maximum value of 3.07‰ at 0.725 m. In subunit G, the fluctuation of $\delta^{13}C$ values has stabilized. It has an average value of ~2.30‰ with a minimum value of 1.87‰ at 1.73 m and a maximum value of 2.58‰ at 1.71 m. The three uppermost samples, just below the top-Loka unconformity are taken at 1.84 m, 1.845 m and at 1.87 m and have $\delta^{13}C$ values of 2.53‰, 2.49‰ and 2.31‰, respectively. At the unconformity, sample DSU31 is taken roughly three millimetres above the unconformity and has a value of 1.79‰. Sample SU-71 is taken roughly 0.5 cm above the unconformity and has a value of 2.31‰. Sample DSU-32 is taken roughly one cm above the unconformity and has a value of 1.17‰, which is at the baseline of the Motala Formation. Hence, there is an offset of more than 1.00‰ between samples separated by only 0.5 cm, adding evidence for a hiatus associated with the unconformity at the top of the Loka Formation.

Based on the dense sampling of the HICE-interval, four broad trends or clusters of $\delta^{13}C$ values can be discerned and these help to define significant and likely statistically solid changes in the HICE trend (Fig. 10). The clusters have been defined qualitatively based on their increasing or decreasing trends in $\delta^{13}C$ values or because of exceptional scattering of data.

The initial rise of the HICE has been studied in particular detail to understand how $\delta^{13}C$ values correspond to different microfacies, and to evaluate if the microfacies, which may represent different environments and/or processes, have any potential impact on these values. The $\delta^{13}C$ values in the lower part of the Loka Formation (-0.16 m to 0.34 m) represent sampling from four different carbonate microfacies. The

microfacies constitutes; 1) lithoclasts with similar wackestone-packstone microfacies as in the upper Jonstorp, that is, reworked strata (lithoclasts are distributed within subunits A-C); 2) packstone-grainstone matrix in the basal reworked facies (subunit A); 3) pure packstone-grainstone sets of the laminated facies (subunit B); and 4) laminated packstone-grainstone sets, separated by laminae mixed with quartz-rich organic mudstone (subunit B). The $\delta^{13}C$-records of the four microfacies are plotted together in Figure 11. It is notable but expected that the lithoclasts with a similar microfacies as upper Jonstorp generally have lower values than the other three microfacies. As the $\delta^{13}C$ values steadily increase initiating the rising limb of the HICE in the basal Loka Formation, these data behave steadier and appear to display an increasing offset to the rising limb up-section, adding evidence for a reworked origin from older strata. The packstone-grainstone matrix in subunit A shows an increasing trend that upwards is sustained by the two microfacies of the laminated facies. The graph also shows that the values between individual depositional sets in the laminated subunit B are changing, not always increasing upwards from one set to the next although with a general trend of increasing upwards. This also means that the many thin depositional sets in subunit B did not form due to flow-regime changes during one single depositional event, but that the sets were deposited one -by-one, separated by some significant amount of time. A few values within each plot change close to the uncertainty of the method, although the trends remain.

### 6.3 Post-HICE

Within the Motala Formation (1.90 m to 3.71 m) 28 $\delta^{13}C$ samples were analysed (Fig. 3). Directly following the unconformity at the base the values return to a baseline of ~1.20‰. From 3.55 m the values start to increase and at 3.7 m values reach 1.71‰ just below the flooding surface that marks the transition into the Silurian. Within the Silurian mudstone (3.7 m to 11.09 m) 51 $\delta^{13}C$ samples were analysed. At 3.76 m, above the basal flooding surface the value is 1.76‰ followed by an immediate drop to 0.79‰ at 3.8 m. The values continue to slowly decrease from ~0.90‰ to ~0.40‰ and the last and uppermost value of 0.37‰ is recorded at 10.9 m.

## 7 Discussion

### 7.1 The Upper Ordovician of the Stora Sutarve core

Among the most significant stratigraphic markers, of the Stora Sutarve core, are the thirteen bentonite beds in the Kahula Formation (Fig. 3). These are most likely including the Kinnekulle bentonite (e.g. Bergström et al., 2011; Bergström, Lehnert, et al., 2012) of Upper Sandbian age although it cannot be properly identified in the core without further study. Above the last bentonite bed, is the Hirmuse Formation, which includes fissures filled with coarse spar, herein interpreted as freshwater diagenesis due to exposure of the succession. The Hirmuse formation is also characterized by *Planolites* trace fossils and a series of stacked mineralized hardgrounds (Fig. 5B). The Rägavere Formation above is characterized by abundant calcareous algae of the genus *Vermiporella.* The overlying Paekna Formation is characterized by a high abundance of detrital glauconite. The Slandrom Formation and its Estonian counterpart Saunja Formation, which are widespread at this stratigraphic level, is missing in the Stora Sutarve core. Their typical fine-grained (aphanitic) facies has not been encountered in the core. Commonly, the black, organic-rich (oil shale) Fjäcka Shale follows above the Slandrom Formation. No black shale is, however, found in the Stora Sutarve core at this stratigraphic level. Instead the glauconite-rich Paekna Formation is followed immediately by the Jonstorp Formation. As been noted above, however, the lowermost portion of the lower member of the Jonstorp Formation interfingers with a dark-coloured mudstone, which is here provisionally interpreted as a Fjäcka Shale equivalent. The lower Jonstorp member is overlain by the conspicuous Öglunda Limestone (Figs. 4F and 5C). This is a porous biohermal limestone (boundstone) with abundant calcareous algae of the genus *Dasyporella.* Hydrocarbons are present in the pore spaces. The upper Jonstorp member shows a typical Jonstorp facies. The Loka Formation of Hirnantian age follows above with reworked clasts of similar microfacies as the upper member of the Jonstorp Formation. The Loka Formation continues with conspicuously laminated limestone (Figs. 6A and 7B-C). The lower Skultorp Member includes a brachiopod coquina (Figs. 6E and 7F-G) at the top boundary to the upper member. The following upper member is clay rich and includes a darker interval. The carbonate content increase upwards in the upper member and the formation ends in an unconformity at the upper boundary which inferably marks the Silurian boundary. Above the Loka Formation is the Motala Formation, which ends in a flooding surface. A mudstone belonging to the Kallholn Formation follows on top of the Motala Formation and continuous to the end of the studied core.

### 7.2 Upper Ordovician carbon isotope stratigraphy

The $\delta^{13}C$ isotope excursions identified in the studied section includes the LSNICE, the GICE, the Moe excursion, the HICE and an excursion associated with the flooding surface at the inferred Ordovician-Silurian boundary (Fig. 3). Approximately between -21.90 m to -19.32 m, in between the bentonite beds in the Kahula Formation, is a pronounced negative excursion with a minimum value of -0.76‰ at -20.50 m which likely corresponds to the LSNICE, although the LSNICE occurs somewhat stratigraphically lower in the Tartu-453 core (Bauert et al., 2014). At the Sandbian GSSP in the Fågelsång valley east of Lund, the LSNICE has been identified between bentonite beds (Bergström, Kleffner, et al., 2020) similar to the Stora Sutarve core. The trend of increasing $\delta^{13}C$ values above the LSNICE from -19.52 has been designated the GICE. The rising limb of this excursion occurs within the uppermost meter of the Kahula Formation, which includes three bentonite beds. It continues into the Hirmuse Formation where a distinct decrease from 0.51‰ to -0.17‰ in the $\delta^{13}C$ values is interpreted as a truncation and erosion of strata, although it is not by any means obvious in the lithology. The GICE thus

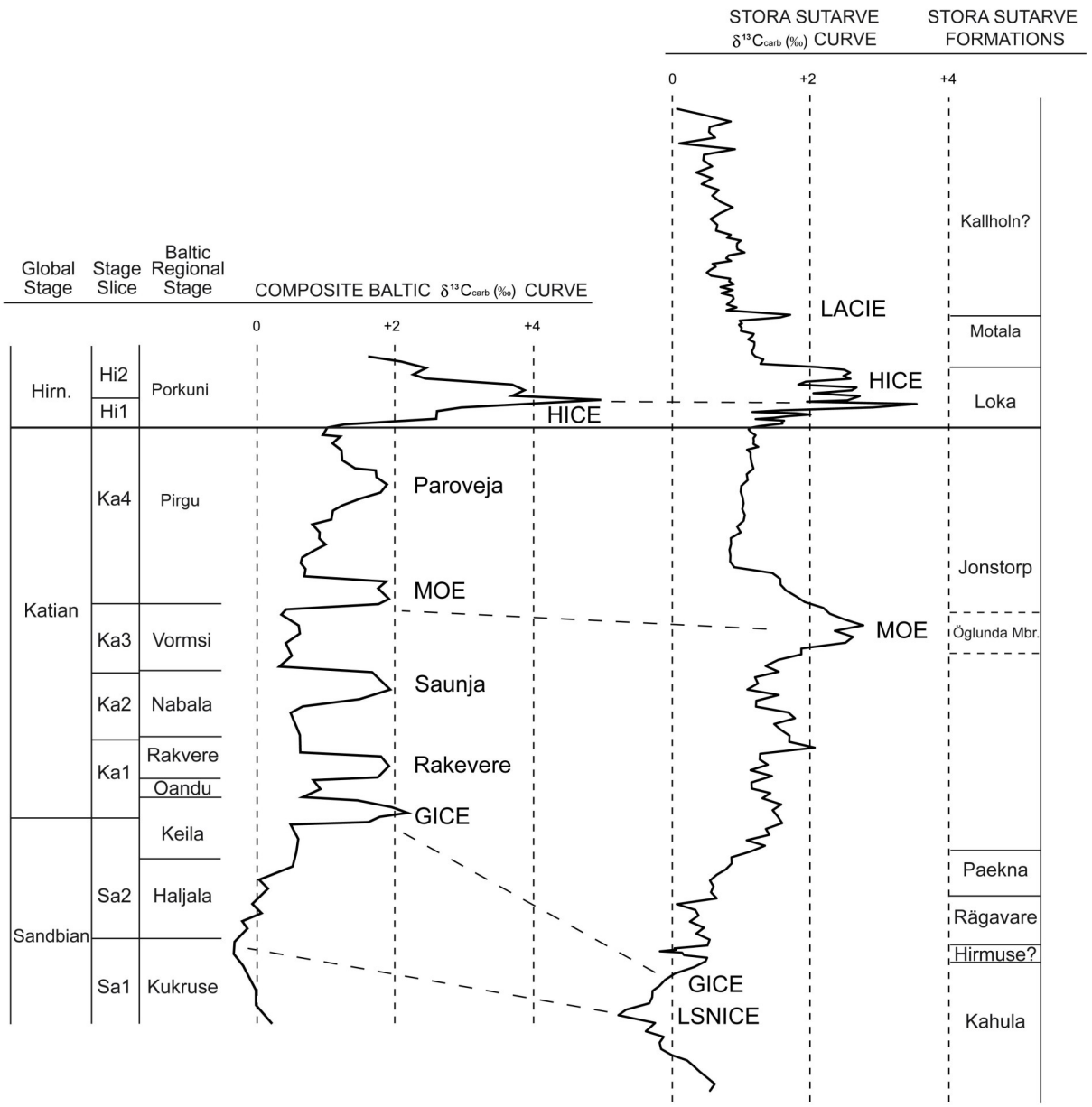


*Fig. 12.* To the left, stratigraphy and a composite $\delta^{13}C$ curve of the Baltic Upper Ordovician based on fig 7. from Ainsaar et al. (2010). This is compared with the herein established $\delta^{13}C$ curve from the Stora Sutarve core, including the identified $\delta^{13}C$ excursions.

occurs among the top three bentonite beds in the Kinnekulle bentonite complex, similar to what has been reported elsewhere in the Baltoscandian basin (Ainsaar et al., 2010; Bauert et al., 2014; Bergström, Lehnert, et al., 2012; O. Hints et al., 2014). The Rakvere excursion is associated with the Rägavere Formation (Rakvere regional stage) but no isotope excursion is identified in the Rägavere Formation of the Stora Sutarve core. The Rägavere and Paekna formations are separated by an unconformity but this is not noticeable in the $\delta^{13}C$ values, although the Rägavere excursion could be in the missing strata of the hiatus. $\delta^{13}C$ values of the Paekna Formation (Nabala regional stage) show an increase to a higher baseline of values. This increase might be part of a broader trend and is not pronounced enough to confidently be assigned to the Saunja excursion which is associated with the Nabala regional stage. In the lower member of the Jonstorp Formation, there is an increase in $\delta^{13}C$ values from 1.28‰ to 2.07‰ between -11.54 m and -11.31 m, which might be due to the fact that the high $\delta^{13}C$ value is derived from a more calcareous nodule. The subsequent $\delta^{13}C$ values continues at a slightly higher baseline around ~1.70‰, but nothing notable occurs in the lithology that is associated with the increase or the increased baseline. Similarly an increase of $\delta^{13}C$ values is documented in the lower member of that formation in the Borenshult core (Bergström, Lehnert, et al., 2012), although much less pronounced. The middle member of the Jonstorp Formation, the Öglunda Limestone includes a pronounced positive $\delta^{13}C$ excursion. This excursion is designated as the Moe excursion based on its stratigraphic position and similarities with the associated Moe For-

mation. This excursion is initiated slightly below the Öglunda Limestone in the lower member of the Jonstorp Formation, and the decreasing falling limb of the excursion continues upwards in the above lying upper member of the Jonstorp Formation. The upwards following part of the upper member of the Jonstorp Formation shows the least fluctuating values of this study. In Baltoscandia, the Paroveja excursion has been identified within this stratigraphic interval (Ainsaar et al., 2010) but there is no such excursion in the Stora Sutarve core.

In the Loka Formation of Hirnantian age, the HICE has been identified (Figs. 3 and 10). The unconformable lower contact is not obvious in the HICE as the $\delta^{13}C$ values steadily increase across boundary between upper Jonstorp and the Loka Formation. A significant jump to the highest $\delta^{13}C$ values is seen within in subunit C, slightly below the quartz-rich subunit D. A cluster of high values, including the peak value of 3.54‰ within the coquina, continues to the end of subunit E. The fluctuation of $\delta^{13}C$ values seen in the clay-rich subunit F is interpreted as diagenetic effects. Lithologies rich in clay mineral or organic rich mud may during diagenesis have released carbon of low $\delta^{13}C$, which would have decreased the $\delta^{13}C$ in the carbonate rock. As the carbonate increases upwards, the $\delta^{13}C$ values stabilize in a funnelling pattern. The stabilized values continue in subunit G and a plateau can be interpreted from subunit E to G if the diagenetic fluctuation is disregarded. The HICE ends with a truncation corresponding to the unconformity seen in the core and the falling limb is missing. The high-resolution at which this study was carried out, highlights that substantial variation in values can occur depending on sample site, such as sampling from reworked clasts or spar-filled bioclasts. The high sample density not only made the general trends of the HICE clearer but also the diagenetic fluctuation as seen in subunit F. The rising limb of the HICE is inferably not microfacies dependent based on the comparison between different microfacies in Figure 11. The microfacies did not differ substantially from each other in $\delta^{13}C$ values except the slightly lower $\delta^{13}C$ values of reworked upper Jonstorp clasts. A tripartite morphology can be discerned if the inferred diagenetic fluctuation in subunit F is disregarded. The rising limb is confined to subunit A – C. The plateau continues from subunit D-G, with a peak in subunit E, whereas the falling limb is not preserved as the HICE is truncated at the unconformity.

In the Motala Formation immediately above the top unconformity of the Loka Formation the $\delta^{13}C$ values return to baseline (Fig. 10). Slightly below a flooding surface, which inferably marks the boundary to the Kallholn Formation, another excursion occurs (Fig. 3). This excursion is truncated back to baseline values slightly above the flooding surface. This excursion could correspond to the Late Aeronian CIE (Melchin & Holmden, 2006), inferring that Early Aeronian strata are missing in a hiatus associated with the flooding surface at the top of the Motala Formation. Biostratigraphic data, however, are necessary to assert this. The excursions of the Stora Sutarve core are presented in Figure 12 along with a composite $\delta^{13}C$ curve of the Baltic Upper Ordovician based on Ainsaar et al. (2010) for comparison.

## 7.3 Hirnantian eustatic sea-level change and the Loka Formation

The Hirnantian Stage is often interpreted in terms of sea-level change due to the glacio-eustasy of the Hirnantian glaciation. This is often difficult, however, due to the lack of conformable successions, which is also the case with the Stora Sutarve record. In this interpretation (Fig. 13) terms from sequence stratigraphy are used, including; Falling stage systems tract (FSST), Lowstand systems tract (LST), Transgressive systems tract (TST), Highstand systems tract (HST) and Maximum Flooding Interval (MFI).

The reworked Jonstorp clasts in subunit A imply that the Jonstorp-Loka contact is unconformable although no distinct erosional surface is obvious from the core section and no offset in the isotope stratigraphy is detected. The implied, minor stratigraphic gap may represent the initial glaciation of the Hirnantian Stage. Any strata belonging to the FSST would thus be eroded and not preserved in the area of the coring. Likewise could the LST strata be eroded away or be located further palaeo-offshore. The reworked clasts appear to be exclusively of upper Jonstorp origin. They are common especially in subunits A and B and continue with less abundance up to subunit C. The concentration of clasts at lower levels and their successive decrease up-section suggest they were first reworked and redeposited during a transgression. This trend is associated with an upwards overall increase in clay minerals to reach a maximum abundance of clay in the lower portions of subunit F. Here, a dark clay inferably marks the MFI of the transgression and the top of the clay thus marks the top of the TST. The TST therefore is represented by subunits A, B, C, D, E and lowermost part of F. Such subdivision of the strata may explain the isotopic offset associated with the subunit C-D transition as related to transgressive erosion and a development of a transgressive ravinement surface. Above the dark clay, subunit F shows a gradually increased content of carbonate upwards. This trend may mirror an increased carbonate production in the area due to progradation of the shoreline and fit with a normal regression associated with the HST. The transition from subunit F to G is gradual and the facies change represents a shallowing upwards. The unconformity at the top subunit G then is interpreted as the second FSST, which herein is interpreted as corresponding to the second glacial on Gondwana. It is likely that part of the HST is also not fully represented below the unconformity but partly eroded away. The Loka Formation in the Stora Sutarve core is thus interpreted as one transgression-regression cycle bounded by two glacially induced hiatuses at the base and top. This interpretation can be contrasted with the recent study of Kiipli & Kiipli (2020; figs 7-9). They identified four regressions ($I\text{-}IV_R$) and three transgressions ($II\text{-}IV_T$), all within the Hirnantian Stage. Consequently, several of their cycles are either not sufficiently pronounced or not developed in the Stora Sutarve record. Below two scenarios are introduced that may explain this difference.

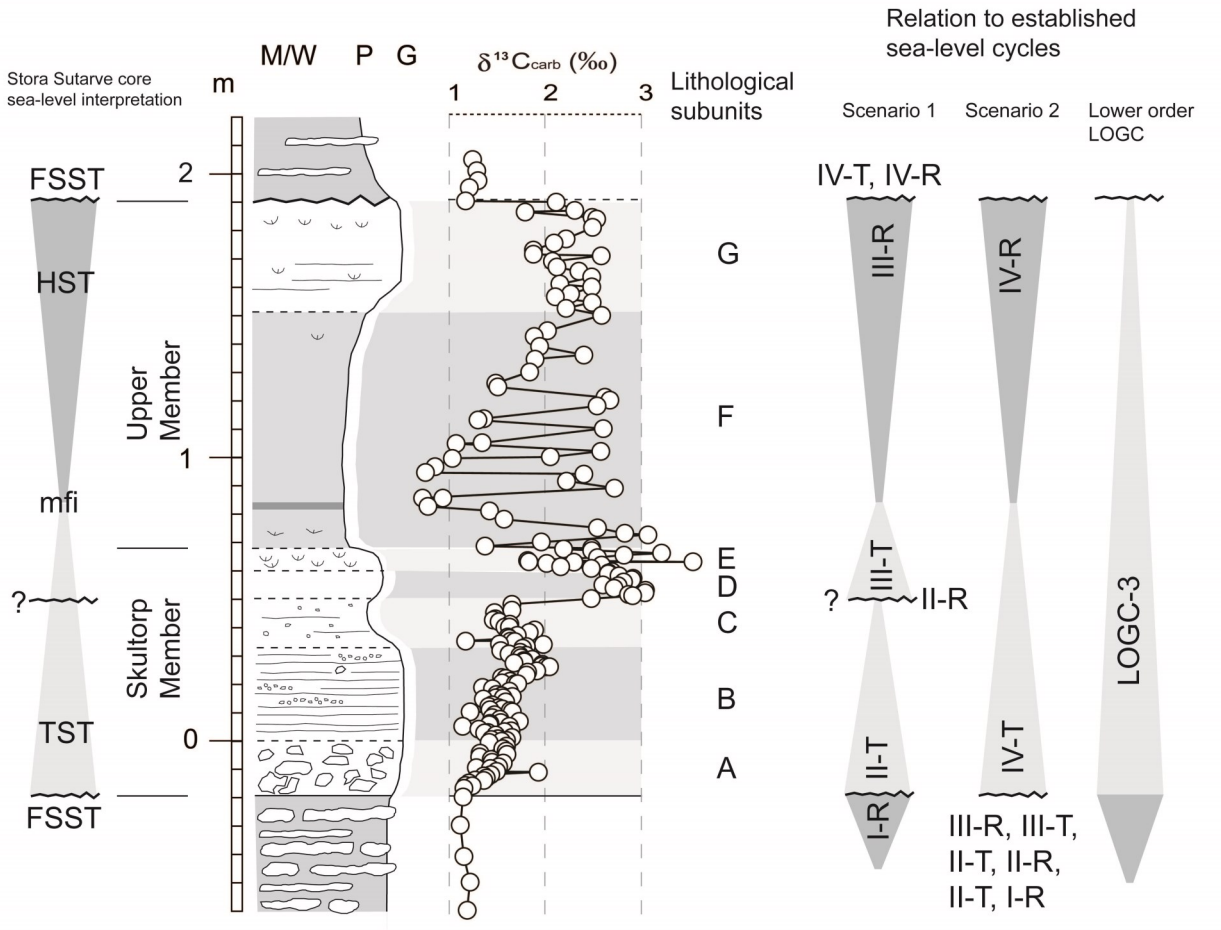


*Fig. 13.* Lithology and the HICE of the Loka Formation in the Stora Sutarve core. To the left is the sea-level interpretation proposed herein based on the lithology, facies and HICE of the Stora Sutarve core. To the right are two scenarios where the sea-level interpretation is compared to the Hirnantian Baltic regression-transgression cycles proposed by Kiipli and Kiipli (2020). Furthest to the right is the proposed relation to the lower order LOGC cycles of Ghienne et al. (2014). FSST = Falling stage system tract, TST = transgressive system tract, mfi = maximum flooding interval, HST = Highstand system tract. In the top of the log is the Dunham classification for carbonate sedimentary rocks M/W = mudstone/wackestone, P = packstone, G = grainstone. I-R = the earliest regression in the Hirnantian Baltic regression-transgression cycles proposed by Kiipli and Kiipli (2020), IV-R = the latest regression, II-T = the earliest transgression, IV-T = the latest transgression. LOGC = Late Ordovician Glacial Cycle from Ghienne et al. (2014). ? = the herein interpreted transgressive ravinement surface that in Scenario 1 is interpreted as an erosional surface.

Scenario 1

One possible indication of an additional period of sea-level lowstand and erosion in the Stora Sutarve record is the more than one per mille offset in the $\delta^{13}C$ values associated with the boundary between subunits C and D. This surface is here interpreted as a local ravinement surface. Below and above this offset the $\delta^{13}C$ values cluster in widely different ranges (Fig. 10) and this offset thus could indicate the presence of an erosional surface, thus a regressive-transgressive cycle (Fig. 13). $II_T$ of Kiipli & Kiipli (2020) could then correlate with subunits A-C of the Skultorp Member. The $\delta^{13}C$ offset would then represent a hiatus formed during $II_R$, possibly including the quartz-rich subunit D. Subsequently $III_T$ follows in the brachiopod coquina (subunit E) up to the MFI in subunit F. The following highstand in subunit F is assigned to $III_R$. The unconformity at the top of subunit G represents $IV_T$ and $IV_R$, which are both eroded due to Stora Sutarve subaerial palaeoposition during $IV_R$. This scenario thus includes strata from the earlier cycles in the Stora Sutarve record, which would develop when the regressive coastline stands were less offset from Southern Gotland. Whereas strata deposited during the late $IV_T$ could erode to a greater extent as the regressive coastline stand was further out in the basin during $IV_R$. Another interpretation, however, is that the isotopic offset is related to transgressive erosion as discussed above.

Scenario 2

Another explanation is that the time corresponding to some of the sea-level cycles proposed by Kiipli & Kiipli (2020) is included in the hiatus at the base of the Loka Formation, which requires a different sea-level interpretation, here denoted scenario 2. Harper & Hints (2016) correlated the Loka Formation in the Borenshult core with the Saldus Formation in the East Baltic area. The Skultorp Member of the Loka Formation would then be the equivalent of the Piltene Member of the Saldus Formation, and the upper member of the

Loka Formation would correspond to the Broceni Member. Based on the similarities between the Borenshult and Stora Sutarve cores, such correlation can be assumed to apply to the Stora Sutarve core as well. The Piltene Member of the Saldus Formation belongs to the so called Saldus transgression $IV_T$ of Kiipli & Kiipli (2020), which would imply that the Skultorp Member (both in Stora Sutarve core and in the Borenshult core) formed during transgression $IV_T$ (Fig. 13). The Broceni Member corresponds to regression $IV_R$ (Kiipli & Kiipli, 2020) and inferably to the upper member or possibly only the unconformity at the top of the Loka Formation. $III_R$ and all the previous cycles would in this scenario be represented by the hiatus at the base of the Loka Formation. This could explain the lack of the lowermost member of the Loka Formation known from Västergötland (Stridsberg, 1980) and Östergötland (Bergström et al., 2011; Bergström & Bergström, 1996), although a missing lower member is a bit surprising given the seemingly steady $\delta^{13}C$ values across this boundary. The scenario fits better with the Borenshult core, which has a distinct unconformity and an associated offset in $\delta^{13}C$ values across the base of the Loka Formation. If the regressive coastline stand is taken into account, as shown in Kiipli & Kiipli (2020; fig. 8), it would be more logical if the basal Loka Formation was preserved whereas the top would be eroded away, as in scenario 1, as more of the Baltoscandian basin was exposed to land.

Lower order cyclicity

The lower order glacial cycles LOGC-1 and LOGC-2 from Anticosti Island (Ghienne et al., 2014), are older than cycles identified in the Baltoscandian basin as these include the *Belonechitina gamachiana* chitinozoan Zone (Ghienne et al., 2014; Kiipli & Kiipli, 2020). The Hirnantian in the Baltoscandian basin starts in the slightly younger *S. taugourdeuai* chitinozoan Zone and matches with LOGC-3 (Kiipli & Kiipli, 2020). The LOGC-3 also matches with the peak of HICE. The peak of the HICE is associated with the rising sea-level in the deglaciation (Ghienne et al., 2014). The HICE of the Stora Sutarve core starts and peaks within a TST and the plateau continues through an interval of normal regression interpreted as a HST (Fig. 13). This would imply that the unconformity at the top of the Loka Formation is not another glacial episode but a regional hiatus due to a regionally confined regression. A major glacial episode should occur earlier in LOGC-3 (Ghienne et al., 2014), which could be represented by the conglomeratic and unconformable lower boundary of the Loka Formation in the Stora Sutarve core and the corresponding basal unconformity of the Loka Formation in the Borenshult core.

The rise and peak of the HICE in the Stora Sutarve core is associated with a TST, most likely transgression $IV_T$ of Kiipli & Kiipli (2020), and the plateau interval continues in a HST. Ghienne et al., (2014) argues that the peak of HICE always occurs within the TST of LOGC-3 and at higher resolution in a HST, which is associated with the post-glacial warming and deglaciation. If this is the case, the weathering hypothesis of Kump et al (1999), would be refuted as it requires the peak within a lowstand (Ghienne et al., 2014). The record of the Stora Sutarve core is thus not in line with the weathering hypothesis, although the Stora Sutarve record is a single core and global investigation of multiple cores would be necessary to further a dismissal of the weathering hypothesis.

## 7.4 An assessment of the brachiopod fauna

Several brachiopods of both the *Hirnantia* and the Edgewood-Cathay faunas have been identified in the Loka Formation (Fig. 9). *Hindella* of the *Hirnantia* fauna and *Brevilamnulella kjerulfi* of the succeeding Edgewood-Cathay fauna do not, as would be supposed, occur consecutively. Instead they co-occur, in the coquina of subunit E and throughout subunit G including the second coquina. By comparison the Hirnantian Boda Limestone includes a *Hindella* coquina associated with the peak of the HICE and a *Brevilamnulella* coquina associated with the falling limb of the HICE just below the upper hiatus (Kröger et al., 2015, fig. 4) and in the Hirnantian Langøyene Formation in Norway, a *Brevilamnulella* coquina also occurs near below the upper unconformity of the formation (Brenchley & Cocks, 1982; see also Calner et al., 2021). Notably the lowermost identified brachiopod in the Stora Sutarve core is *Parastrophina* of the Edgewood-Cathay fauna. If the subdivision of transitional benthic faunas (Wang et al., 2019) is applied, the TBF do not occur consecutively. *Kinnella* of TBF-1 occurs both in the first coquina and in the upper part of subunit F. *Hindella* and *Parastrophina* of TBF-2 occur both in the first coquina and throughout the uppermost subunit G. *Brevilamnulella* of TBF-3 also occurs in the first coquina and throughout subunit G.

## 7.5 Regional correlation of HICE

The Loka Formation in the Borenshult core (Bergström et al., 2011; Bergström, Lehnert, et al., 2012) is lithologically similar to the Stora Sutarve core as they both have oolitic laminated limestone in the lower part (Skultorp Member) and a muddier upper member which increases in carbonate content upwards. Both cores have unconformable upper and lower boundaries. In the Borenshult core the boundary between the Skultorp Member and the upper member was interpreted as unconform and assigned the designation HA (Bergström, Lehnert, et al., 2012). In this study, which includes an inspection of the Borenshult core for comparison, an unconformable boundary at this level was not observed neither is it obvious in the $\delta^{13}C$ values. Both cores are located in the same Central Baltoscandian Confacies Belt. The most obvious differences between the cores are observed in the rising limb of the respective HICE (Fig. 14). The Stora Sutarve core displays a steady increase whereas the Borenshult core displays an offset associated with the basal unconformity. Furthermore, the Borenshult core displays a more stable peak and plateau than the Stora Sutarve core. Both cores have the most pronounced fluctuation in $\delta^{13}C$ values in the upper members, likely due to the intake of carbon, low in $\delta^{13}C$, from clay-minerals or organic-rich mud during diagenesis. To aid the visual comparison of the cores, many of the $\delta^{13}C$ values in Stora Sutarve has been excluded in Figure 14.

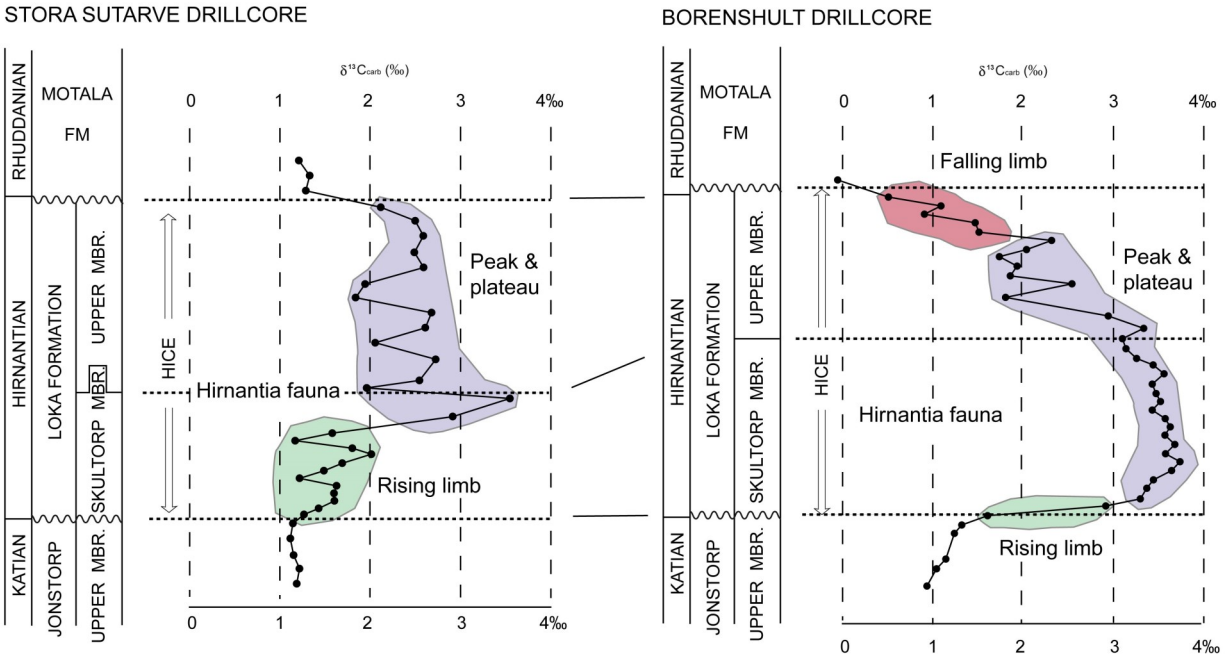


*Fig. 14.* HICE of the Stora Sutarve core compared to the HICE of the Borenshult core. Many of the $\delta^{13}C$ values have been omitted from the Stora Sutarve core for better visualization, the general morphology remains the same. The rising limb of the HICE is marked in green, the peak and plateau is marked in blue and the falling limb is marked in red.

The Hirnantian Stage (Porkuni regional stage) in the Viki core constitutes the Ärina Formation and the Saldus Formation. The lithology, compared to the Loka Formation of the Stora Sutarve core is generally different as the Viki core drill site is positioned in the margins of another confacies belt (Fig. 2). The peak of HICE is confined to the oolitic Piltene Member in the Viki core (O. Hints et al., 2014). This member was correlated to the Skultorp Member in the Borenshult core by Harper & Hints (2016). Comparably, the peak of HICE occurs in the topmost part of the Skultorp Member in the Stora Sutarve core. A plateau and falling limb occur in the Broceni Member in the Viki core (O. Hints et al., 2014) which was correlated to the upper member in the Borenshult core (Harper & Hints, 2016). In the Stora Sutarve core, if the fluctuation of $\delta^{13}C$ values in the upper member is disregarded, a plateau emerges, which is subsequently truncated before a falling limb can be discerned.

# 8 Conclusions

Based on lithological characterization and carbon isotope stratigraphy this study summarizes the Upper Ordovician stratigraphy of the Stora Sutarve core from southern Gotland, with particular focus on the sedimentology, isotope stratigraphy and palaeontology of the Hirnantian Stage. In total 391 whole-rock carbon isotope samples were analysed from the core. Of these, 189 samples were from the 2.09 m thick Loka Formation. The following are the key results and conclusions of the study.

1) The 34.50 m long core section ranges stratigraphically from the Sandbian Kahula Formation to the Aeronian Kallholn Formation.
2) A $\delta^{13}C$ stratigraphy has been established for the entire stratigraphic interval. Several of the globally known Upper Ordovician $\delta^{13}C$ excursions have been identified for the first time in the Gotland area; LSNICE, GICE, Moe excursion, HICE and possibly the Late Aeronian ICE
3) A high-resolution record of the HICE is evaluated. It includes a rising limb, a peak and a plateau interval, whereas the falling limb is cut off at an unconformity at the top of the Loka Formation. The rise and peak of the HICE occur in a TST and the plateau interval continues in the overlying HST. Based on the dense sampling four clusters of $\delta^{13}C$ values help to define significant changes in the HICE trend. Based on study of carbonate microfacies and $\delta^{13}C$ values from the Loka Formation, the $\delta^{13}C$ values of the rising limb are inferred to be microfacies-independent except for the reworked clasts of Jonstorp origin. A significant offset is seen at the HICE transition from the rising limb to the peak cluster. This offset may be due to transgressive erosion, rather than erosion during a sea-level lowstand.
4) Brachiopods of the *Hirnantia* and the Edgewood-Cathay faunas have been identified within the Loka Formation. The specific genera of the two faunas co-occur, however, and do not appear consecutively as would be expected.
5) Changes in sea-level have been interpreted and compared to previously published regression-transgression cycles in the Baltic (Kiipli & Kiipli, 2020) and on Anticosti Island (Ghienne et al., 2014). The Loka Formation corresponds to one cycle of transgression-

regression bounded by two unconformities, inferably resulting from glacio-eustasy. The cycle has been fitted into two possible scenarios (Fig. 13) relating to the Baltic regression-transgression cycles of Kiipli and Kiipli (Kiipli & Kiipli, 2020). The cycle has also been fitted into the LOGC-3 of Ghienne et al. (Ghienne et al., 2014).

6) The Hirnantian Stage in the core has been compared to the Borenshult core (Bergström et al., 2011; Bergström, Lehnert, et al., 2012) and to the Viki core (O. Hints et al., 2014; Põldvere, 1998). The lithology of the Loka Formation is similar to the Borenshult core. The HICE also shows similarities although the most pronounced difference is the steady rising limb in the Stora Sutarve core compared to the large off-set in the rising limb in the Borenshult core.

# 9 Acknowledgements

First and foremost I would like to acknowledge and thank my supervisor Mikael Calner for support, guidance and interesting discussions throughout this project. I would also like to thank Rongchang Wu at the Nanjing Institute of Geology and Palaeontology, for the many analyses of $\delta^{13}C$ samples. I am grateful to Christian Rasmussen at the Globe Institute at the University of Copenhagen, for the help with identification of brachiopods and interesting discussions about the Hirnantian Stage. Thanks should also go to Oliver Lehnert and the team at Friedrich-Alexander University Erlangen-Nurnberg, in Erlangen, for the production of thin sections. I would also like to thank Linn Valtonen and Frans Lundberg for the earlier $\delta^{13}C$ sampling in the core, previous to the start of this project. And thanks to Anders Lindskog at Lund University for help and good advice. And lastly thanks to Peter Dahlqvist and Mikael Erlström at SGU for access to the core.

# 10 References

Achab, A., Asselin, E., Desrochers, A., Riva, J. F., & Farley, C. (2011). Chitinozoan biostratigraphy of a new Upper Ordovician stratigraphic framework for Anticosti Island, Canada. *GSA Bulletin*, *123*(1–2), 186–205. https://doi.org/10.1130/B30131.1

Ainsaar, L., Kaljo, D., Martma, T., Meidla, T., Männik, P., Nõlvak, J., & Tinn, O. (2010). Middle and Upper Ordovician carbon isotope chemostratigraphy in Baltoscandia: A correlation standard and clues to environmental history. *Palaeogeography, Palaeoclimatology, Palaeoecology*, *294*(3), Article 3. https://doi.org/10.1016/j.palaeo.2010.01.003

Amberg, C., Collart, T., Salenbien, W., Egger, L., Munnecke, A., Nielsen, A., Monnet, C., Hammer, O., & Vandenbroucke, T. (2016). The nature of Ordovician limestone-marl alternations in the Oslo-Asker District (Norway): Witnesses of primary glacio-eustasy or diagenetic rhythms? *Scientific Reports*, *6*, 18787. https://doi.org/10.1038/srep18787

Bauert, H., Ainsaar, L., Põldsaar, K., & Sepp, S. (2014). Δ13C chemostratigraphy of the Middle and Upper Ordovician succession in the Tartu-453 drillcore, southern Estonia, and the significance of the HICE. *Estonian Journal of Earth Sciences*, *63*(4), Article 4. https://doi.org/10.3176/earth.2014.18

Bergström, S. M., & Bergström, J. (1996). The Ordovician-Silurian boundary successions in östergötland and Västergötland, S. Sweden. *GFF*, *118*(1), Article 1. https://doi.org/10.1080/11035899609546227

Bergström, S. M., Calner, M., Lehnert, O., & Noor, A. (2011). A new upper Middle Ordovician–Lower Silurian drillcore standard succession from Borenshult in Östergötland, southern Sweden: 1. Stratigraphical review with regional comparisons. *GFF*, *133*(3–4), Article 3–4. https://doi.org/10.1080/11035897.2011.622049

Bergström, S. M., Eriksson, M. E., Schmitz, B., Young, S. A., & Ahlberg, P. (2016). Upper Ordovician δ13Corg chemostratigraphy, K-bentonite stratigraphy, and biostratigraphy in southern Scandinavia: A reappraisal. *Palaeogeography, Palaeoclimatology, Palaeoecology*, *454*, 175–188. https://doi.org/10.1016/j.palaeo.2016.04.037

Bergström, S. M., Eriksson, M. E., Young, S. A., Ahlberg, P., & Schmitz, B. (2014). Hirnantian (latest Ordovician) δ13C chemostratigraphy in southern Sweden and globally: A refined integration with the graptolite and conodont zone successions. *GFF*, *136*(2), Article 2. https://doi.org/10.1080/11035897.2013.851734

Bergström, S. M., Eriksson, M. E., Young, S. A., & Widmark, E.-M. (2012). Conodont biostratigraphy, and δ13C and δ34S isotope chemostratigraphy, of the uppermost Ordovician and Lower Silurian at Osmundsberget, Dalarna, Sweden. *GFF*, *134*(4), 251–272. https://doi.org/10.1080/11035897.2012.758169

Bergström, S. M., Kleffner, M., & Eriksson, M. E. (2020). Upper Katian (Upper Ordovician) trans-Atlantic δ13C chemostratigraphy: The geochronological equivalence of the ELKHORN and PAROVEJA excursions and its implications. *Lethaia*, *53*(2), Article 2. https://doi.org/10.1111/let.12351

Bergström, S. M., Lehnert, O., Calner, M., & Joachimski, M. M. (2012). A new upper Middle Ordovician–Lower Silurian drillcore standard succession from Borenshult in Östergötland, southern Sweden: 2. Significance of δ13C chemostratigraphy. *GFF*, *134*(1), Article 1. https://doi.org/10.1080/11035897.2012.657231

Bergström, S. M., Saltzman, M. M., & Schmitz, B. (2006). First record of the Hirnantian (Upper Ordovician) $\delta^{13}C$ excursion in the North American Midcontinent and its regional implications. *Geological Magazine*, *143*(5), Article 5. https://doi.org/10.1017/S0016756806002469

Bergström, S. M., Schmitz, B., Terfelt, F., Eriksson, M. E., & Ahlberg, P. (2020). The $\delta^{13}C$ chemostratigraphy of Ordovician global stage stratotypes: Geochemical data from the Floian and Sandbian GSSPs in Sweden. *GFF*, *142*(1), 23–

32. https://doi.org/10.1080/11035897.2019.1631883

Bergström, S. M., Young, S., & Schmitz, B. (2010). Katian (Upper Ordovician) δ13C chemostratigraphy and sequence stratigraphy in the United States and Baltoscandia: A regional comparison. *Palaeogeography, Palaeoclimatology, Palaeoecology*, *296*(3), Article 3. https://doi.org/10.1016/j.palaeo.2010.02.035

Berner, R. A. (1990). Atmospheric Carbon Dioxide Levels Over Phanerozoic Time. *Science*, *249* (4975), Article 4975.

Berry, W. B. N., Quinby-Hunt, M. S., & Wilde, P. (1995). Impact of Late Ordovician Glaciation-Deglaciation on Marine Life. In Studies in Geophysics: EVects of Past Global Change on Life, 34-46. In *Effects of Past Global Change on Life*. National Academies Press (US). https://www.ncbi.nlm.nih.gov/books/NBK231940/

Brenchley, P. J. (2004). 9. End Ordovician Glaciation. In B. D. Webby, F. Paris, M. L. Droser, & I. G. Percival (Eds.), *The Great Ordovician Biodiversification Event* (pp. 81–83). Columbia University Press. https://doi.org/10.7312/webb12678-010

Brenchley, P. J., Carden, G. A., Hints, L., Kaljo, D., Marshall, J. D., Martma, T., Meidla, T., & Nõlvak, J. (2003). High-resolution stable isotope stratigraphy of Upper Ordovician sequences: Constraints on the timing of bioevents and environmental changes associated with mass extinction and glaciation. *Geological Society of America Bulletin*, *115*(1), Article 1. https://doi.org/10.1130/0016-7606(2003)115<0089:HRSISO>2.0.CO;2

Brenchley, P. J., & Cocks, L. (1982). Ecological associations in a regressive sequence: The latest Ordovician of the Oslo-Asker district, Norway. *Palaeontology*. https://www.semanticscholar.org/paper/Ecological-associations-in-a-regressive-sequence%3A-Brenchley-Cocks/c6573783e9203d45a2a1774871061544ba09e599

Brenchley, P. J., Marshall, J. D., Carden, G. A. F., Robertson, D. B. R., Long, D. G. F., Meidla, T., Hints, L., & Anderson, T. F. (1994). Bathymetric and isotopic evidence for a short-lived Late Ordovician glaciation in a greenhouse period. *Geology*, *22*(4), Article 4. https://doi.org/10.1130/0091-7613(1994)022<0295:BAIEFA>2.3.CO;2

Calner, M., Bockelie, J. F., Rasmussen, C. M. Ø., Calner, H., Lehnert, O., & Joachimski, M. M. (2021). Carbon isotope chemostratigraphy and sea-level history of the Hirnantian Stage (uppermost Ordovician) in the Oslo-Asker district, Norway. *Geological Magazine*, *158*(11), Article 11. https://doi.org/10.1017/S0016756821000546

Calner, M., Lehnert, O., & Nõlvak, J. (2010). Palaeokarst evidence for widespread regression and subaerial exposure in the middle Katian (Upper Ordovician) of Baltoscandia: Significance for global climate. *Palaeogeography, Palaeoclimatology, Palaeoecology*, *296*(3), Article 3. https://doi.org/10.1016/j.palaeo.2009.11.028

Chen, X., Rong, J., Fan, J., Zhan, R., Mitchell, C., Harper, D., Melchin, M., Ping'an, P., Finney, S., & Wang, X. (2006). The Global Boundary Stratotype Section and Point (GSSP) for the base of the Hirnantian Stage (the uppermost of the Ordovician System). *Episodes*, *29*, 183–195. https://doi.org/10.18814/epiiugs/2006/v29i3/004

Crowley, T. J., & Baum, S. K. (1991). Toward reconciliation of Late Ordovician (~440 Ma) glaciation with very high CO2 levels. *Journal of Geophysical Research: Atmospheres*, *96*(D12), Article D12. https://doi.org/10.1029/91JD02449

Ebbestad, J. O. R., Högström, A. E. S., Frisk, Å. M., Martma, T., Kaljo, D., Kröger, B., & Pärnaste, H. (2015). Terminal Ordovician stratigraphy of the Siljan district, Sweden. *GFF*, *137*(1), Article 1. https://doi.org/10.1080/11035897.2014.945620

Fan, J., Peng, P., & Melchin, M. J. (2009). Carbon isotopes and event stratigraphy near the Ordovician–Silurian boundary, Yichang, South China. *Palaeogeography, Palaeoclimatology, Palaeoecology*, *276*(1), 160–169. https://doi.org/10.1016/j.palaeo.2009.03.007

Finney, S. C., Berry, W. B. N., Cooper, J. D., Ripperdan, R. L., Sweet, W. C., Jacobson, S. R., Soufiane, A., Achab, A., & Noble, P. J. (1999). Late Ordovician mass extinction: A new perspective from stratigraphic sections in central Nevada. *Geology*, *27*(3), 215–218. https://doi.org/10.1130/0091-7613(1999)027<0215:LOMEAN>2.3.CO;2

Ghienne, J.-F., Desrochers, A., Vandenbroucke, T. R. A., Achab, A., Asselin, E., Dabard, M.-P., Farley, C., Loi, A., Paris, F., Wickson, S., & Veizer, J. (2014). A Cenozoic-style scenario for the end-Ordovician glaciation. *Nature Communications*, *5*(1), Article 1. https://doi.org/10.1038/ncomms5485

Gradstein, F. M., Ogg, J. G., Schmitz, M. D., & Ogg, G. M. (Eds.). (2020). Title page. In *Geologic Time Scale 2020* (pp. i–iii). Elsevier. https://doi.org/10.1016/B978-0-12-824360-2.00032-2

Hammarlund, E. U., Dahl, T. W., Harper, D. A. T., Bond, D. P. G., Nielsen, A. T., Bjerrum, C. J., Schovsbo, N. H., Schönlaub, H. P., Zalasiewicz, J. A., & Canfield, D. E. (2012). A sulfidic driver for the end-Ordovician mass extinction. *Earth and Planetary Science Letters*, *331–332*, 128–139. https://doi.org/10.1016/j.epsl.2012.02.024

Harper, D. A. T., Hammarlund, E. U., & Rasmussen, C. M. Ø. (2014). End Ordovician extinctions: A coincidence of causes. *Gondwana Research*, *25* (4), Article 4. https://doi.org/10.1016/j.gr.2012.12.021

Harper, D. A. T., & Hints, L. (2016). Hirnantian (Late Ordovician) brachiopod faunas across Baltoscandia: A global and regional context. *Palaeogeography, Palaeoclimatology, Palaeoecology*, *444*, 71–83. https://doi.org/10.1016/j.palaeo.2015.11.044

Harris, M. T., Sheehan, P. M., Ainsaar, L., Hints, L., Männik, P., Nõlvak, J., & Rubel, M. (2004). Upper Ordovician sequences of western Estonia. *Palaeogeography, Palaeoclimatology, Palaeoecology*, *210*(2), 135–148. https://doi.org/10.1016/j.palaeo.2004.02.045

Hints, L., Oraspold, A., & Nolvak, J. (2005). The Pirgu Regional Stage (Upper Ordovician) in the East Baltic; lithostratigraphy, biozonation, and correlation. *Proceedings of the Estonian Academy of Sciences, Geology = Eesti Teaduste Akadeemia Toimetised, Geoloogia*, *54*(4), 225–259.

Hints, O., Martma, T., Männik, P., Nõlvak, J., Põldvere, A., Shen, Y., & Viira, V. (2014). New data on Ordovician stable isotope record and conodont biostratigraphy from the Viki reference drill core, Saaremaa Island, western Estonia. *GFF*, *136*(1), 100–104. https://doi.org/10.1080/11035897.2013.873989

Jaanusson, V. (1973). Aspects of carbonate sedimentation in the Ordovician of Baltoscandia. *Lethaia*, *6*(1), 11–34. https://doi.org/10.1111/j.1502-3931.1973.tb00871.x

Jaanusson, V. (1982). *The Siljan district. In D.L. Bruton & S.H. Williams (eds.):IV. International Symposium on the Ordovician System. Field excursion guide* (pp. 15–42). Palaeontological Contributionsfrom the University of Oslo.

Jaanusson, V. (1995). CONFACIES DIFFERENTIATION AND UPPER MIDDLE ORDOVICIAN CORRELATION IN THE BALTOSCANDIAN BASIN. *Proceedings of the Estonian Academy of Sciences. Geology*, *44*(2), Article 2. https://doi.org/10.3176/geol.1995.2.01

Jablonski, D. (1991). Extinctions: A Paleontological Perspective. *Science*, *253*(5021), Article 5021. https://doi.org/10.1126/science.253.5021.754

Jones, D. S., Fike, D. A., Finnegan, S., Fischer, W. W., Schrag, D. P., & McCay, D. (2011). Terminal Ordovician carbon isotope stratigraphy and glacioeustatic sea-level change across Anticosti Island (Québec, Canada). *GSA Bulletin*, *123*(7–8), 1645–1664. https://doi.org/10.1130/B30323.1

Kiipli, E., & Kiipli, T. (2020). Hirnantian sea-level changes in the Baltoscandian Basin, a review. *Palaeogeography, Palaeoclimatology, Palaeoecology*, *540*, 109524. https://doi.org/10.1016/j.palaeo.2019.109524

Kröger, B., Ebbestad, J. O. R., Lehnert, O., Ullmann, C. V., Korte, C., Frei, R., & Rasmussen, C. M. Ø. (2015). Subaerial speleothems and deep karst in central Sweden linked to Hirnantian glaciations. *Journal of the Geological Society*, *172*(3), 349–356. https://doi.org/10.1144/jgs2014-071

Kröger, B., Penny, A., Shen, Y., & Munnecke, A. (2019). Algae, calcitarchs and the Late Ordovician Baltic limestone facies of the Baltic Basin. *Facies*, *66*(1), 1. https://doi.org/10.1007/s10347-019-0585-0

Kump, L. R., Arthur, M. A., Patzkowsky, M. E., Gibbs, M. T., Pinkus, D. S., & Sheehan, P. M. (1999). A weathering hypothesis for glaciation at high atmospheric pCO2 during the Late Ordovician. *Palaeogeography, Palaeoclimatology, Palaeoecology*, *152*(1), Article 1. https://doi.org/10.1016/S0031-0182(99)00046-2

Lefebvre, V., Servais, T., François, L., & Averbuch, O. (2010). Did a Katian large igneous province trigger the Late Ordovician glaciation?: A hypothesis tested with a carbon cycle model. *Palaeogeography, Palaeoclimatology, Palaeoecology*, *296*(3), Article 3. https://doi.org/10.1016/j.palaeo.2010.04.010

Ling, M.-X., Zhan, R.-B., Wang, G.-X., Wang, Y., Amelin, Y., Tang, P., Liu, J.-B., Jin, J., Huang, B., Wu, R.-C., Xue, S., Fu, B., Bennett, V. C., Wei, X., Luan, X.-C., Finnegan, S., Harper, D. A. T., & Rong, J.-Y. (2019). An extremely brief end Ordovician mass extinction linked to abrupt onset of glaciation. *Solid Earth Sciences*, *4*(4), Article 4. https://doi.org/10.1016/j.sesci.2019.11.001

Longman, J., Mills, B. J. W., Manners, H. R., Gernon, T. M., & Palmer, M. R. (2021). Late Ordovician climate change and extinctions driven by elevated volcanic nutrient supply. *Nature Geoscience*, *14*(12), Article 12. https://doi.org/10.1038/s41561-021-00855-5

Melchin, M. J., & Holmden, C. (2006). Carbon isotope chemostratigraphy of the Llandovery in Arctic Canada: Implications for global correlation and sea-level change. *GFF*, *128*(2), 173–180. https://doi.org/10.1080/11035890601282173

Männik, P., Loydell, D. K., Nestor, V., & Nõlvak, J. (2015). Integrated Upper Ordovician–lower Silurian biostratigraphy of the Grötlingbo-1 core section, Sweden. *GFF*, *137*(3), Article 3. https://doi.org/10.1080/11035897.2015.1042032

Page, A. a. ( 1, 2 ), Zalasiewicz, J. a. ( 1 ), Williams, M. ( 1 ), & Popov, L. e. ( 3 ). (2007). Were transgressive black shales a negative feedback modulating glacioeustasy in the Early Palaeozoic Icehouse? In *Deep-Time Perspectives on Climate Change: Marrying the Signal from Computer Models and Biological Proxies* (p. 156). Geological Society of London. https://doi.org/10.1144/tms002.6

Pohl, A., Donnadieu, Y., Le Hir, G., Buoncristiani, J.-F., & Vennin, E. (2014). Effect of the Ordovician paleogeography on the (in)stability of the climate. *Climate of the Past*, *10*(6), 2053–2066. https://doi.org/10.5194/cp-10-2053-2014

Põldvere, A. (1998). Estonian geological sections. Viki drilll core. *Geological Survey of Estonia Bulletin 10*, 1–56.

Poussart, P. F., Weaver, A. J., & Barnes, C. R. (1999). Late Ordovician glaciation under high atmospheric CO2: A coupled model analysis. *Paleoceanography*, *14*(4), 542–558. https://doi.org/10.1029/1999PA900021

Ripperdan, R. L., Cooper, J. D., & Firmey, S. R. (1998). High-resolution 813C and lithostratigraphic profiles from Copenhagen Canyon, Nevada: Clues to the behaviour of ocean carbon during the Late Ordovician global crisis. *Mineralogical Magazine*, *62A*, 1279–1280.

Rong, J., Harper, D. A. T., Huang, B., Li, R., Zhang,

X., & Chen, D. (2020). The latest Ordovician Hirnantian brachiopod faunas: New global insights. *Earth-Science Reviews*, *208*, 103280. https://doi.org/10.1016/j.earscirev.2020.103280

Schmitz, B., & Bergström, S. M. (2007). Chemostratigraphy in the Swedish Upper Ordovician: Regional significance of the Hirnantian δ13C excursion (HICE) in the Boda Limestone of the Siljan region. *GFF*, *129*(2), Article 2. https://doi.org/10.1080/11035890701292133

Sheehan, P. M. (2001). The Late Ordovician mass extinction. *Annual Review of Earth and Planetary Sciences*, *29*, 331–364.

Stridsberg, S. (1975). *Sedimentology of upper Ordovician regressive strata in Västergötland* (Geobiblioteket). http://ludwig.lub.lu.se/login?url=https://search.ebscohost.com/login.aspx?direct=true&AuthType=ip,uid&db=cat07147a&AN=lub.1735150&site=eds-live&scope=site

Stridsberg, S. (1980). Sedimentology of upper ordovician regressive strata in västergötland. *GFF*, *102*(3), 213–221. Scopus. https://doi.org/10.1080/11035898009455160

Sutcliffe, O. E., Dowdeswell, J. A., Whittington, R. J., Theron, J. N., & Craig, J. (2000). Calibrating the Late Ordovician glaciation and mass extinction by the eccentricity cycles of Earth's orbit. *Geology*, *28*(11), 967–970. https://doi.org/10.1130/0091-7613(2000)28<967:CTLOGA>2.0.CO;2

Suzuki, Y., Shiino, Y., & Bergström, J. (2009). Stratigraphy, carbonate facies and trilobite associations in the Hirnantian part of the Boda Limestone, Sweden. *GFF*, *131*(4), 299–310. https://doi.org/10.1080/11035890903452670

Wang, G., Zhan, R., & Percival, I. G. (2019). The end-Ordovician mass extinction: A single-pulse event? *Earth-Science Reviews*, *192*, 15–33. https://doi.org/10.1016/j.earscirev.2019.01.023

Williams, G. E. (1991). Milankovitch-band cyclicity in bedded halite deposits contemporaneous with Late Ordovician-Early Silurian glaciation, Canning Basin, Western Australia. *Earth and Planetary Science Letters*, *103*(1), 143–155. https://doi.org/10.1016/0012-821X(91)90156-C

Zou, C., Qiu, Z., Poulton, S. W., Dong, D., Wang, H., Chen, D., Lu, B., Shi, Z., & Tao, H. (2018). Ocean euxinia and climate change "double whammy" drove the Late Ordovician mass extinction. *Geology*, *46*(6), Article 6. https://doi.org/10.1130/G40121.1

## **Appendix A** (below)

Photographs of the studied 34.5 m of the core from core boxes 81-86.

## **Appendix B** (to the right)

Core scans of the Loka Formation with $\delta^{13}C$ values plotted to the right. $\delta^{13}C$ sample sites are marked with circles in the core scans. White circle are samples taken from the frontal sawed surfaced and grey circles are samples taken from the back of the core. Grey lines to the left of the core represent studied thin sections.

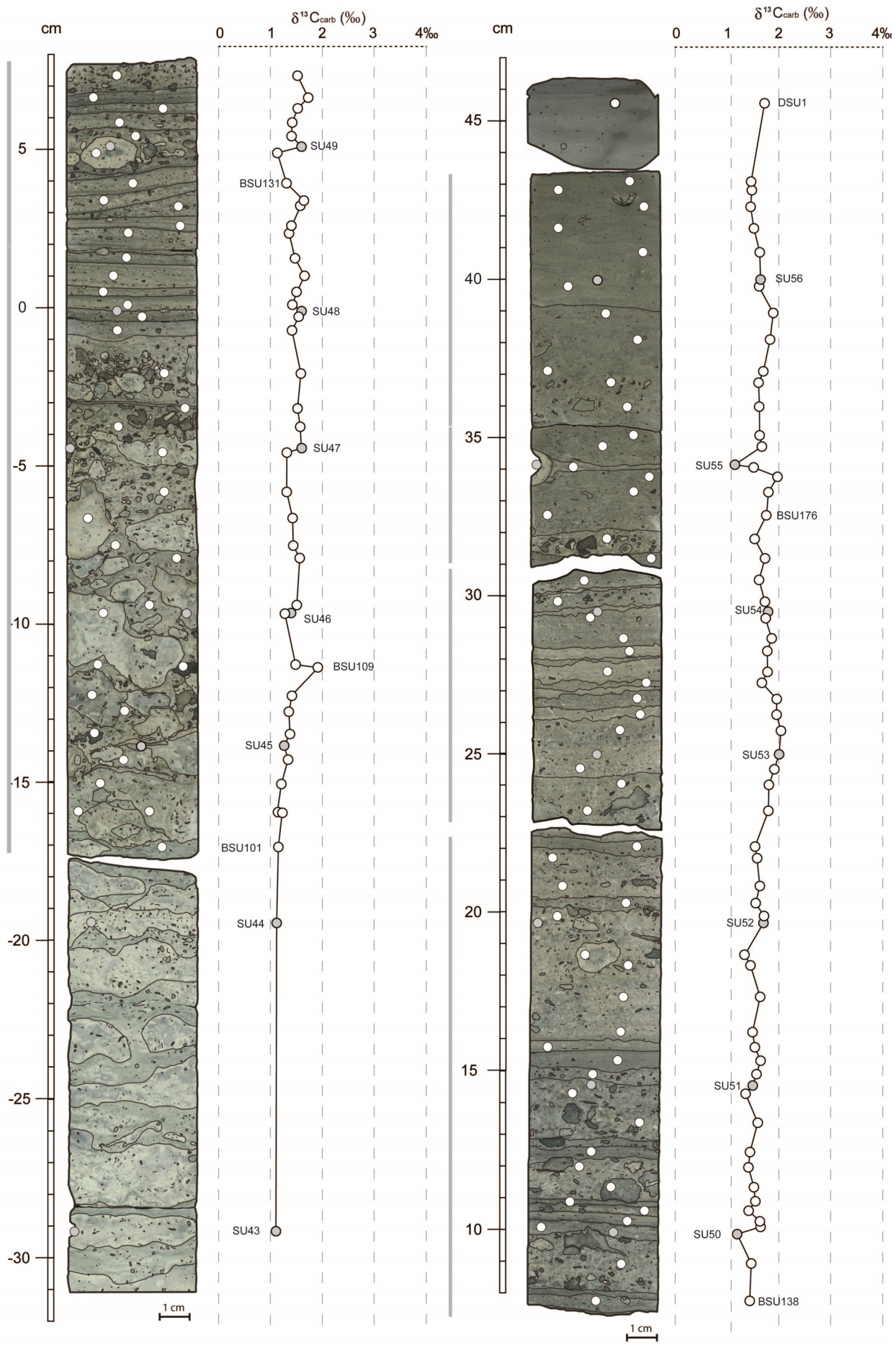
cm
δ13Ccarb (‰)
0
1
2
3
4‰
5
0
-5
-10
-15
-20
-25
-30
SU49
BSU131
SU48
SU47
SU46
BSU109
SU45
BSU101
SU44
SU43
1 cm
cm
δ13Ccarb (‰)
0
1
2
3
4‰
45
40
35
30
25
20
15
10
DSU1
SU56
SU55
BSU176
SU54
SU53
SU52
SU51
SU50
BSU138
1 cm

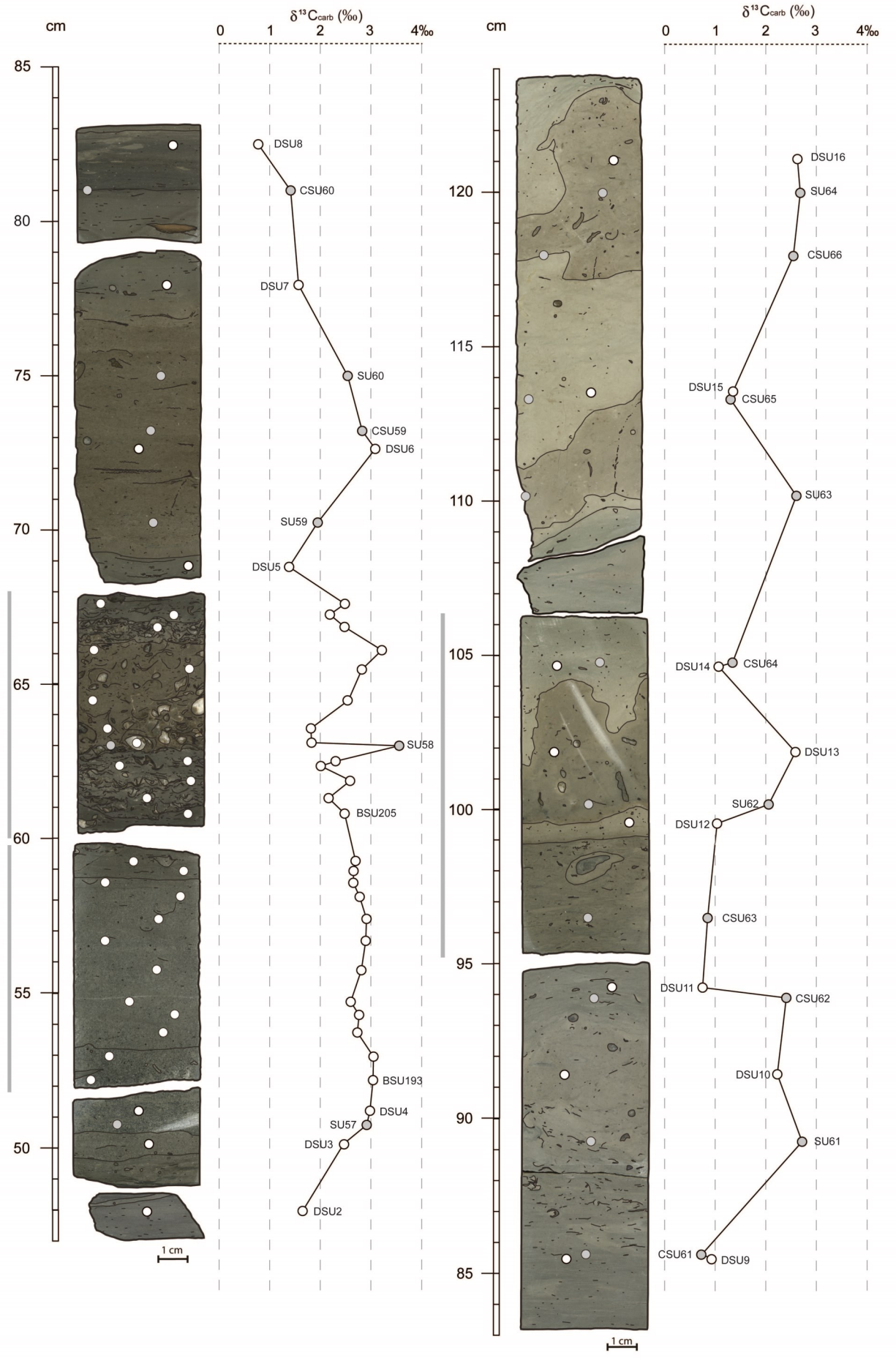
cm
δ13Ccarb (‰)
0
1
2
3
4‰
85
80
75
70
65
60
55
50
DSU8
CSU60
DSU7
SU60
CSU59
DSU6
SU59
DSU5
SU58
BSU205
BSU193
DSU4
SU57
DSU3
DSU2
1 cm
cm
δ13Ccarb (‰)
0
1
2
3
4‰
120
115
110
105
100
95
90
85
DSU16
SU64
CSU66
DSU15
CSU65
SU63
DSU14
CSU64
DSU13
SU62
DSU12
CSU63
DSU11
CSU62
DSU10
SU61
CSU61
DSU9
1 cm

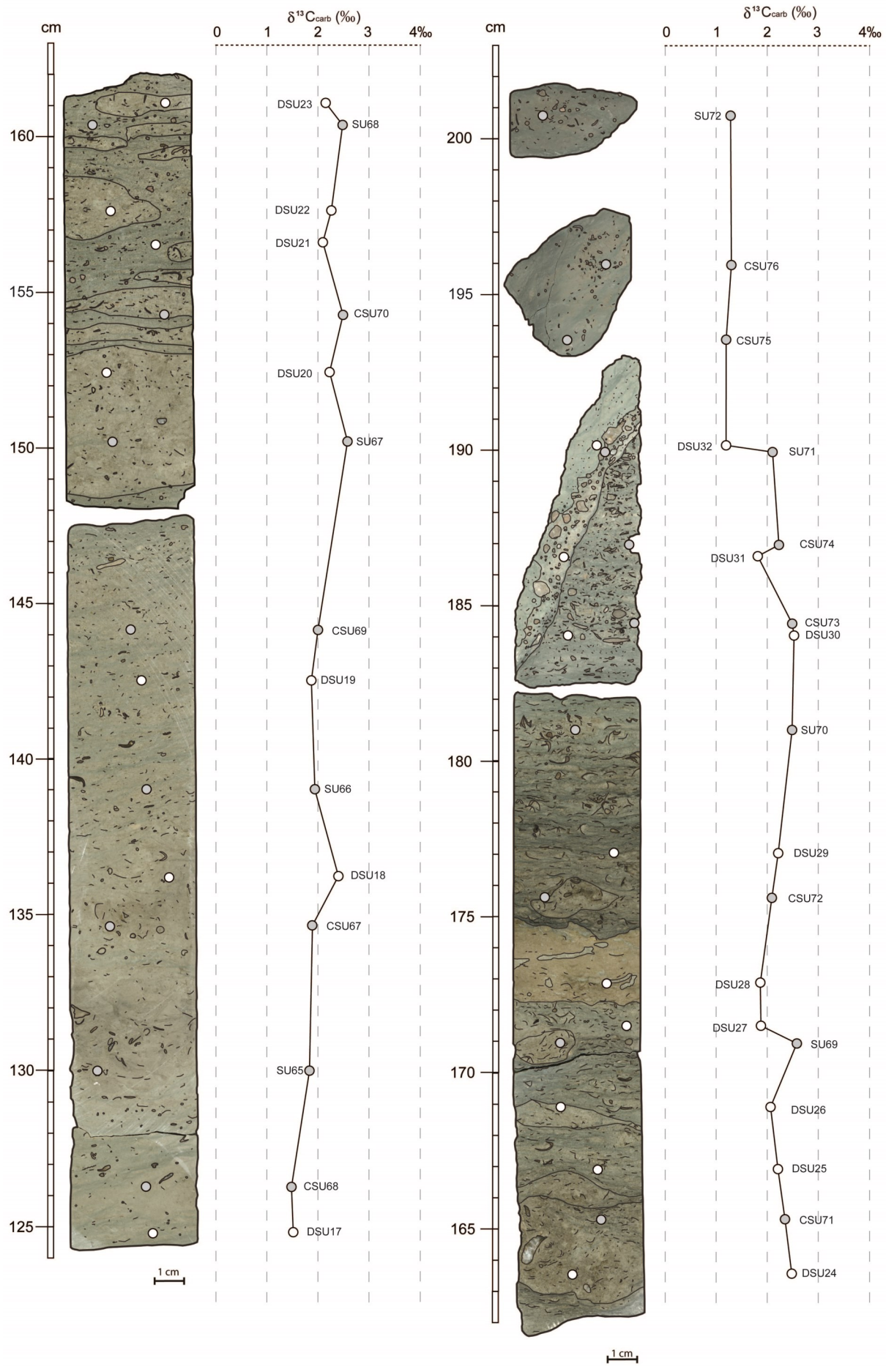
cm
δ13Ccarb (‰)
0
1
2
3
4‰
160
155
150
145
140
135
130
125
DSU23
SU68
DSU22
DSU21
CSU70
DSU20
SU67
CSU69
DSU19
SU66
DSU18
CSU67
SU65
CSU68
DSU17
1 cm
200
195
190
185
180
175
170
165
SU72
CSU76
CSU75
DSU32
SU71
CSU74
DSU31
CSU73
DSU30
SU70
DSU29
CSU72
DSU28
DSU27
SU69
DSU26
DSU25
CSU71
DSU24
1 cm

# Appendix C

Table of $\delta^{13}C$ values from the Stora Sutarve core with information about values sample-id, sampling depth and from which formation the samples were taken.

| Sample-id | Formation | Depth (m) | $\delta^{13}C$ (‰) |
|---|---|---|---|
| CSU-58 | Kahula | -23.16 | 0.55 |
| CSU-57 | Kahula | -22.92 | 0.62 |
| CSU-56 | Kahula | -22.70 | 0.52 |
| CSU-55 | Kahula | -22.50 | 0.41 |
| CSU-54 | Kahula | -22.26 | 0.31 |
| CSU-53 | Kahula | -22.09 | 0.22 |
| CSU-52 | Kahula | -21.90 | 0.00 |
| CSU-51 | Kahula | -21.73 | -0.15 |
| CSU-50 | Kahula | -21.48 | -0.18 |
| CSU-49 | Kahula | -21.29 | -0.12 |
| CSU-48 | Kahula | -21.08 | -0.38 |
| CSU-47 | Kahula | -20.90 | -0.24 |
| CSU-46 | Kahula | -20.50 | -0.78 |
| CSU-45 | Kahula | -20.38 | -0.66 |
| CSU-44 | Kahula | -20.12 | -0.33 |
| CSU-43 | Kahula | -19.94 | -0.28 |
| CSU-42 | Kahula | -19.69 | -0.28 |
| CSU-41 | Kahula | -19.52 | -0.18 |
| CSU-40 | Kahula | -19.32 | -0.10 |
| CSU-39 | Kahula | -19.12 | 0.04 |
| CSU-38 | Kahula | -18.88 | 0.32 |
| CSU-37 | Hirmuse | -18.67 | 0.49 |
| CSU-36 | Hirmuse | -18.48 | 0.51 |
| CSU-86 | Hirmuse | -18.430 | 0.18 |
| CSU-35 | Hirmuse | -18.30 | 0.15 |
| CSU-85 | Hirmuse | -18.260 | -0.17 |
| CSU-84 | Hirmuse | -18.200 | 0.06 |
| CSU-83 | Rägavere | -18.150 | 0.04 |
| CSU-34 | Rägavere | -18.12 | 0.51 |
| CSU-33 | Rägavere | -17.94 | 0.55 |
| CSU-32 | Rägavere | -17.73 | 0.35 |
| CSU-31 | Rägavere | -17.52 | 0.46 |
| CSU-30 | Rägavere | -17.33 | 0.26 |
| CSU-29 | Rägavere | -17.10 | 0.38 |
| CSU-28 | Rägavere | -16.90 | 0.34 |
| CSU-27 | Rägavere | -16.72 | 0.07 |
| CSU-26 | Rägavere | -16.51 | 0.65 |
| CSU-25 | Paekna | -16.30 | 0.57 |
| CSU-24 | Paekna | -16.10 | 0.60 |
| CSU-23 | Paekna | -15.90 | 0.55 |
| CSU-22 | Paekna | -15.70 | 0.65 |
| CSU-21 | Paekna | -15.50 | 0.78 |
| CSU-20 | Paekna | -15.31 | 0.87 |
| CSU-19 | Paekna | -15.10 | 0.86 |
| CSU-18 | Paekna | -14.90 | 1.14 |
| CSU-17 | Jonstorp | -14.70 | 1.35 |
| CSU-16 | Jonstorp | -14.50 | 1.08 |
| CSU-15 | Jonstorp | -14.32 | 1.41 |
| CSU-14 | Jonstorp | -14.12 | 1.36 |
| CSU-13 | Jonstorp | -13.92 | 1.60 |
| CSU-12 | Jonstorp | -13.71 | 1.53 |
| CSU-11 | Jonstorp | -13.46 | 1.46 |
| CSU-10 | Jonstorp | -13.29 | 1.58 |
| CSU-9 | Jonstorp | -13.05 | 1.31 |
| CSU-8 | Jonstorp | -12.87 | 1.43 |
| CSU-7 | Jonstorp | -12.70 | 1.16 |
| CSU-6 | Jonstorp | -12.56 | 1.15 |
| CSU-5 | Jonstorp | -12.28 | 1.45 |
| CSU-4 | Jonstorp | -12.10 | 1.14 |
| CSU-3 | Jonstorp | -11.90 | 1.39 |

| Sample-id | Formation | Depth (m) | $\delta^{13}C$ (‰) | Sample-id | Formation | Depth (m) | $\delta^{13}C$ (‰) |
|---|---|---|---|---|---|---|---|
| CSU-2 | Jonstorp | -11.72 | 1.27 | Su-14 | Jonstorp | -5.29 | 1.45 |
| CSU-1 | Jonstorp | -11.54 | 1.28 | Su-15 | Jonstorp | -5.1 | 0.91 |
| SU-140 | Jonstorp | -11.31 | 2.07 | Su-16 | Jonstorp | -4.91 | 0.84 |
| SU-141 | Jonstorp | -11.12 | 1.70 | Su-17 | Jonstorp | -4.7 | 0.85 |
| SU-142 | Jonstorp | -10.91 | 1.70 | Su-18 | Jonstorp | -4.49 | 0.83 |
| SU-143 | Jonstorp | -10.70 | 1.58 | Su-19 | Jonstorp | -4.3 | 0.86 |
| SU-144 | Jonstorp | -10.50 | 1.48 | Su-20 | Jonstorp | -4.1 | 0.85 |
| SU-145 | Jonstorp | -10.30 | 1.78 | Su-21 | Jonstorp | -3.89 | 1.00 |
| SU-146 | Jonstorp | -10.10 | 1.69 | Su-22 | Jonstorp | -3.7 | 0.94 |
| SU-147 | Jonstorp | -9.90 | 1.22 | Su-23 | Jonstorp | -3.49 | 1.04 |
| SU-148 | Jonstorp | -9.70 | 1.22 | Su-24 | Jonstorp | -3.3 | 1.05 |
| SU-149 | Jonstorp | -9.50 | 1.55 | Su-25 | Jonstorp | -3.09 | 1.02 |
| SU-150 | Jonstorp | -9.31 | 1.09 | Su-26 | Jonstorp | -2.9 | 1.04 |
| SU-151 | Jonstorp | -9.11 | 1.25 | Su-27 | Jonstorp | -2.7 | 1.02 |
| SU-152 | Jonstorp | -8.89 | 1.20 | Su-28 | Jonstorp | -2.49 | 1.00 |
| SU-153 | Jonstorp | -8.70 | 1.54 | Su-29 | Jonstorp | -2.3 | 1.00 |
| SU-154 | Jonstorp | -8.51 | 1.36 | Su-30 | Jonstorp | -2.1 | 1.10 |
| SU-155 | Jonstorp | -8.29 | 1.54 | Su-31 | Jonstorp | -1.9 | 1.08 |
| SU-156 | Jonstorp | -8.10 | 1.87 | Su-32 | Jonstorp | -1.7 | 1.18 |
| Su-1 | Jonstorp | -7.91 | 1.87 | Su-33 | Jonstorp | -1.49 | 1.15 |
| Su-2 | Jonstorp | -7.7 | 2.51 | Su-34 | Jonstorp | -1.31 | 1.14 |
| Su-3 | Jonstorp | -7.5 | 2.62 | Su-35 | Jonstorp | -1.1 | 1.14 |
| Su-4 | Jonstorp | -7.3 | 2.36 | Su-36 | Jonstorp | -1 | 1.09 |
| Su-5 | Jonstorp | -7.09 | 2.77 | Su-37 | Jonstorp | -0.9 | 1.25 |
| Su-6 | Jonstorp | -6.91 | 2.50 | Su-38 | Jonstorp | -0.8 | 1.18 |
| Su-7 | Jonstorp | -6.7 | 2.28 | Su-39 | Jonstorp | -0.7 | 1.18 |
| Su-8 | Jonstorp | -6.5 | 2.19 | Su-40 | Jonstorp | -0.6 | 1.18 |
| Su-9 | Jonstorp | -6.31 | 1.92 | Su-41 | Jonstorp | -0.5 | 1.21 |
| Su-10 | Jonstorp | -6.1 | 1.80 | Su-42 | Jonstorp | -0.41 | 1.15 |
| Su-11 | Jonstorp | -5.9 | 1.65 | Su-43 | Jonstorp | -0.3 | 1.11 |
| Su-12 | Jonstorp | -5.71 | 1.57 | Su-44 | Jonstorp | -0.2 | 1.14 |
| Su-13 | Jonstorp | -5.5 | 1.57 | BSU-101 | Loka | -0.17 | 1.15 |

| Sample-id | Formation | Depth (m) | $\delta^{13}C$ (‰) | Sample-id | Formation | Depth (m) | $\delta^{13}C$ (‰) |
|---|---|---|---|---|---|---|---|
| BSU-102 | Loka | -0.161 | 1.24 | BSU-130 | Loka | 0.034 | 1.64 |
| BSU-103 | Loka | -0.16 | 1.17 | BSU-131 | Loka | 0.039 | 1.30 |
| BSU-104 | Loka | -0.15 | 1.20 | BSU-132 | Loka | 0.049 | 1.14 |
| BSU-105 | Loka | -0.142 | 1.35 | Su-49 | Loka | 0.05 | 1.62 |
| Su-45 | Loka | -0.14 | 1.26 | BSU-133 | Loka | 0.055 | 1.41 |
| BSU-106 | Loka | -0.133 | 1.38 | BSU-134 | Loka | 0.059 | 1.42 |
| BSU-107 | Loka | -0.125 | 1.36 | BSU-135 | Loka | 0.063 | 1.53 |
| BSU-108 | Loka | -0.121 | 1.43 | BSU-136 | Loka | 0.067 | 1.73 |
| BSU-109 | Loka | -0.112 | 1.92 | BSU-137 | Loka | 0.074 | 1.52 |
| BSU-110 | Loka | -0.11 | 1.49 | BSU-138 | Loka | 0.08 | 1.44 |
| Su-46 | Loka | -0.1 | 1.42 | BSU-139 | Loka | 0.09 | 1.47 |
| BSU-111 | Loka | -0.096 | 1.28 | Su-50 | Loka | 0.1 | 1.21 |
| BSU-112 | Loka | -0.093 | 1.51 | BSU-140 | Loka | 0.1 | 1.65 |
| BSU-113 | Loka | -0.08 | 1.56 | BSU-141 | Loka | 0.105 | 1.63 |
| BSU-114 | Loka | -0.078 | 1.44 | BSU-142 | Loka | 0.108 | 1.42 |
| BSU-115 | Loka | -0.067 | 1.43 | BSU-143 | Loka | 0.11 | 1.55 |
| BSU-116 | Loka | -0.058 | 1.31 | BSU-144 | Loka | 0.115 | 1.51 |
| Su-47 | Loka | -0.05 | 1.60 | BSU-145 | Loka | 0.12 | 1.41 |
| BSU-117 | Loka | -0.046 | 1.32 | BSU-146 | Loka | 0.125 | 1.44 |
| BSU-118 | Loka | -0.038 | 1.59 | BSU-147 | Loka | 0.135 | 1.59 |
| BSU-119 | Loka | -0.03 | 1.56 | BSU-148 | Loka | 0.145 | 1.35 |
| BSU-120 | Loka | -0.02 | 1.59 | Su-51 | Loka | 0.15 | 1.48 |
| BSU-121 | Loka | -0.007 | 1.41 | BSU-149 | Loka | 0.15 | 1.56 |
| BSU-122 | Loka | -0.003 | 1.54 | BSU-150 | Loka | 0.154 | 1.65 |
| Su-48 | Loka | 0 | 1.59 | BSU-151 | Loka | 0.158 | 1.54 |
| BSU-123 | Loka | 0.003 | 1.43 | BSU-152 | Loka | 0.162 | 1.49 |
| BSU-124 | Loka | 0.006 | 1.50 | BSU-153 | Loka | 0.173 | 1.63 |
| BSU-125 | Loka | 0.01 | 1.65 | BSU-154 | Loka | 0.182 | 1.45 |
| BSU-126 | Loka | 0.018 | 1.48 | BSU-155 | Loka | 0.187 | 1.34 |
| BSU-127 | Loka | 0.026 | 1.37 | BSU-156 | Loka | 0.199 | 1.71 |
| BSU-128 | Loka | 0.028 | 1.40 | Su-52 | Loka | 0.2 | 1.69 |
| BSU-129 | Loka | 0.031 | 1.57 | BSU-157 | Loka | 0.202 | 1.55 |

| Sample-id | Formation | Depth (m) | $\delta^{13}C$ (‰) | Sample-id | Formation | Depth (m) | $\delta^{13}C$ (‰) |
|---|---|---|---|---|---|---|---|
| BSU-158 | Loka | 0.208 | 1.63 | BSU-187 | Loka | 0.399 | 1.62 |
| BSU-159 | Loka | 0.218 | 1.59 | Su-56 | Loka | 0.4 | 1.58 |
| BSU-160 | Loka | 0.221 | 1.54 | BSU-188 | Loka | 0.41 | 1.63 |
| BSU-161 | Loka | 0.231 | 1.80 | BSU-189 | Loka | 0.418 | 1.52 |
| BSU-162 | Loka | 0.24 | 1.81 | BSU-190 | Loka | 0.424 | 1.45 |
| BSU-163 | Loka | 0.245 | 1.91 | BSU-191 | Loka | 0.429 | 1.48 |
| BSU-164 | Loka | 0.259 | 2.04 | BSU-192 | Loka | 0.451 | 1.47 |
| Su-53 | Loka | 0.26 | 2.01 | DSU-1 | Loka | 0.46 | 1.65 |
| BSU-165 | Loka | 0.262 | 1.96 | DSU-2 | Loka | 0.48 | 1.65 |
| BSU-166 | Loka | 0.268 | 1.96 | DSU-3 | Loka | 0.5 | 2.48 |
| BSU-167 | Loka | 0.272 | 1.67 | Su-57 | Loka | 0.51 | 2.91 |
| BSU-168 | Loka | 0.277 | 1.78 | DSU-4 | Loka | 0.515 | 2.87 |
| BSU-169 | Loka | 0.282 | 1.78 | BSU-193 | Loka | 0.52 | 3.04 |
| BSU-170 | Loka | 0.286 | 1.86 | BSU-194 | Loka | 0.53 | 3.05 |
| BSU-171 | Loka | 0.291 | 1.74 | BSU-195 | Loka | 0.537 | 2.72 |
| BSU-172 | Loka | 0.299 | 1.73 | BSU-196 | Loka | 0.545 | 2.76 |
| Su-54 | Loka | 0.3 | 1.80 | BSU-197 | Loka | 0.549 | 2.60 |
| BSU-173 | Loka | 0.305 | 1.62 | BSU-198 | Loka | 0.559 | 2.81 |
| BSU-174 | Loka | 0.31 | 1.74 | BSU-199 | Loka | 0.568 | 2.90 |
| BSU-175 | Loka | 0.316 | 1.53 | BSU-200 | Loka | 0.572 | 2.91 |
| BSU-176 | Loka | 0.325 | 1.76 | BSU-201 | Loka | 0.581 | 2.77 |
| BSU-177 | Loka | 0.331 | 1.80 | BSU-202 | Loka | 0.588 | 2.65 |
| BSU-178 | Loka | 0.338 | 1.98 | BSU-203 | Loka | 0.59 | 2.66 |
| BSU-179 | Loka | 0.34 | 1.52 | BSU-204 | Loka | 0.595 | 2.69 |
| BSU-180 | Loka | 0.348 | 1.68 | BSU-205 | Loka | 0.607 | 2.48 |
| Su-55 | Loka | 0.35 | 1.17 | BSU-206 | Loka | 0.613 | 2.16 |
| BSU-181 | Loka | 0.35 | 1.63 | BSU-207 | Loka | 0.619 | 2.59 |
| BSU-182 | Loka | 0.36 | 1.62 | BSU-208 | Loka | 0.624 | 2.01 |
| BSU-183 | Loka | 0.365 | 1.61 | BSU-209 | Loka | 0.628 | 2.30 |
| BSU-184 | Loka | 0.37 | 1.70 | Su-58 | Loka | 0.63 | 3.54 |
| BSU-185 | Loka | 0.38 | 1.83 | BSU-210 | Loka | 0.63 | 1.83 |
| BSU-186 | Loka | 0.39 | 1.89 | BSU-211 | Loka | 0.635 | 1.81 |

| Sample-id | Formation | Depth (m) | $\delta^{13}C$ (‰) | Sample-id | Formation | Depth (m) | $\delta^{13}C$ (‰) |
|---|---|---|---|---|---|---|---|
| BSU-212 | Loka | 0.645 | 2.54 | DSU-17 | Loka | 1.247 | 1.50 |
| BSU-213 | Loka | 0.654 | 2.82 | CSU-68 | Loka | 1.260 | 1.48 |
| BSU-214 | Loka | 0.66 | 3.21 | Su-65 | Loka | 1.3 | 1.83 |
| BSU-215 | Loka | 0.67 | 2.48 | CSU-67 | Loka | 1.345 | 1.89 |
| BSU-216 | Loka | 0.675 | 2.19 | DSU-18 | Loka | 1.36 | 2.40 |
| BSU-217 | Loka | 0.678 | 2.48 | Su-66 | Loka | 1.39 | 1.94 |
| DSU-5 | Loka | 0.685 | 1.37 | DSU-19 | Loka | 1.425 | 1.88 |
| DSU-6 | Loka | 0.695 | 3.07 | CSU-69 | Loka | 1.445 | 2.02 |
| Su-59 | Loka | 0.7 | 1.96 | Su-67 | Loka | 1.5 | 2.59 |
| CSU-59 | Loka | 0.730 | 2.83 | DSU-20 | Loka | 1.525 | 2.22 |
| Su-60 | Loka | 0.75 | 2.54 | CSU-70 | Loka | 1.545 | 2.49 |
| DSU-7 | Loka | 0.78 | 1.57 | DSU-21 | Loka | 1.565 | 2.10 |
| CSU-60 | Loka | 0.810 | 1.42 | DSU-22 | Loka | 1.575 | 2.26 |
| DSU-8 | Loka | 0.825 | 0.77 | Su-68 | Loka | 1.6 | 2.48 |
| CSU-61 | Loka | 0.855 | 0.72 | DSU-23 | Loka | 1.61 | 2.15 |
| DSU-9 | Loka | 0.855 | 0.93 | DSU-24 | Loka | 1.635 | 2.48 |
| Su-61 | Loka | 0.89 | 2.72 | CSU-71 | Loka | 1.655 | 2.35 |
| DSU-10 | Loka | 0.915 | 2.22 | DSU-25 | Loka | 1.67 | 2.12 |
| CSU-62 | Loka | 0.940 | 2.40 | DSU-26 | Loka | 1.69 | 2.07 |
| DSU-11 | Loka | 0.945 | 0.75 | Su-69 | Loka | 1.71 | 2.58 |
| CSU-63 | Loka | 0.965 | 0.85 | DSU-27 | Loka | 1.715 | 1.87 |
| DSU-12 | Loka | 0.995 | 1.03 | DSU-28 | Loka | 1.73 | 1.87 |
| Su-62 | Loka | 1 | 2.05 | CSU-72 | Loka | 1.755 | 2.09 |
| DSU-13 | Loka | 1.02 | 2.58 | DSU-29 | Loka | 1.77 | 2.22 |
| DSU-14 | Loka | 1.047 | 1.07 | Su-70 | Loka | 1.81 | 2.49 |
| CSU-64 | Loka | 1.050 | 1.34 | DSU-30 | Loka | 1.84 | 2.53 |
| Su-63 | Loka | 1.1 | 2.61 | CSU-73 | Loka | 1.845 | 2.49 |
| CSU-65 | Loka | 1.130 | 1.30 | DSU-31 | Loka | 1.865 | 1.79 |
| DSU-15 | Loka | 1.135 | 1.35 | CSU-74 | Loka | 1.870 | 2.31 |
| CSU-66 | Loka | 1.180 | 2.54 | Su-71 | Loka | 1.9 | 2.11 |
| Su-64 | Loka | 1.2 | 2.67 | DSU-32 | Motala | 1.903 | 1.17 |
| DSU-16 | Loka | 1.21 | 2.62 | CSU-75 | Motala | 1.950 | 1.20 |

| Sample-id | Formation | Depth (m) | $\delta^{13}C$ (‰) | Sample-id | Formation | Depth (m) | $\delta^{13}C$ (‰) |
|---|---|---|---|---|---|---|---|
| CSU-76 | Motala | 1.975 | 1.30 | Su-97 | Kallholn | 4.5 | 0.88 |
| Su-72 | Motala | 2.01 | 1.28 | Su-98 | Kallholn | 4.6 | 0.71 |
| CSU-77 | Motala | 2.050 | 1.24 | Su-99 | Kallholn | 4.7 | 0.90 |
| Su-73 | Motala | 2.11 | 1.33 | Su-100 | Kallholn | 4.8 | 0.83 |
| Su-74 | Motala | 2.21 | 1.21 | Su-101 | Kallholn | 4.9 | 0.84 |
| Su-75 | Motala | 2.32 | 1.17 | Su-102 | Kallholn | 4.99 | 0.57 |
| Su-76 | Motala | 2.39 | 1.16 | Su-103 | Kallholn | 5.1 | 0.51 |
| Su-77 | Motala | 2.49 | 1.18 | Su-104 | Kallholn | 5.2 | 0.56 |
| Su-78 | Motala | 2.6 | 1.20 | Su-105 | Kallholn | 5.3 | 0.63 |
| Su-79 | Motala | 2.7 | 1.19 | Su-106 | Kallholn | 5.41 | 0.59 |
| Su-80 | Motala | 2.8 | 1.11 | Su-107 | Kallholn | 5.5 | 0.86 |
| Su-81 | Motala | 2.91 | 1.16 | Su-108 | Kallholn | 5.6 | 0.79 |
| Su-82 | Motala | 3 | 1.18 | Su-109 | Kallholn | 5.69 | 0.82 |
| Su-83 | Motala | 3.09 | 1.00 | Su-110 | Kallholn | 5.79 | 1.05 |
| Su-84 | Motala | 3.2 | 1.01 | Su-111 | Kallholn | 5.9 | 0.95 |
| Su-85 | Motala | 3.3 | 0.97 | Su-112 | Kallholn | 6 | 0.94 |
| Su-86 | Motala | 3.4 | 1.01 | Su-113 | Kallholn | 6.1 | 0.94 |
| CSU-78 | Motala | 3.450 | 0.95 | Su-114 | Kallholn | 6.2 | 1.00 |
| Su-87 | Motala | 3.5 | 0.98 | Su-115 | Kallholn | 6.3 | 0.80 |
| CSU-79 | Motala | 3.550 | 1.32 | Su-116 | Kallholn | 6.4 | 0.85 |
| Su-88 | Motala | 3.61 | 1.57 | Su-117 | Kallholn | 6.5 | 0.64 |
| CSU-80 | Motala | 3.635 | 1.56 | Su-118 | Kallholn | 6.7 | 0.66 |
| CSU-81 | Motala | 3.670 | 1.64 | Su-119 | Kallholn | 6.89 | 0.56 |
| Su-89 | Motala | 3.7 | 1.71 | Su-120 | Kallholn | 7.1 | 0.70 |
| CSU-82 | Kallholn | 3.760 | 1.76 | Su-121 | Kallholn | 7.3 | 0.88 |
| Su-90 | Kallholn | 3.8 | 0.79 | Su-122 | Kallholn | 7.5 | 0.70 |
| Su-91 | Kallholn | 3.9 | 0.94 | Su-123 | Kallholn | 7.7 | 0.59 |
| Su-92 | Kallholn | 4 | 0.80 | Su-124 | Kallholn | 7.9 | 0.68 |
| Su-93 | Kallholn | 4.1 | 0.86 | Su-125 | Kallholn | 8.1 | 0.43 |
| Su-94 | Kallholn | 4.2 | 0.89 | Su-126 | Kallholn | 8.3 | 0.59 |
| Su-95 | Kallholn | 4.3 | 0.88 | Su-127 | Kallholn | 8.5 | 0.36 |
| Su-96 | Kallholn | 4.39 | 0.72 | Su-128 | Kallholn | 8.71 | 0.59 |

| Sample-id | Formation | Depth (m) | $\delta^{13}C$ (‰) |
|---|---|---|---|
| Su-129 | Kallholn | 8.91 | 0.45 |
| Su-130 | Kallholn | 9.13 | 0.46 |
| Su-131 | Kallholn | 9.3 | 0.91 |
| Su-132 | Kallholn | 9.5 | 0.11 |
| Su-133 | Kallholn | 9.7 | 0.63 |
| Su-134 | Kallholn | 9.9 | 0.54 |
| Su-135 | Kallholn | 10.11 | 0.55 |
| Su-136 | Kallholn | 10.23 | 0.85 |
| Su-137 | Kallholn | 10.49 | 0.45 |
| Su-138 | Kallholn | 10.69 | 0.08 |
| Su-139 | Kallholn | 10.9 | 0.37 |

## Tidigare skrifter i serien ”Examensarbeten i Geologi vid Lunds universitet”:

594. Johansson, Jonna, 2020: Potentiella nedslagskratrar i Sverige med fokus på Östersjön och östkusten. (15 hp)
595. Haag, Vendela, 2020: Studying magmatic systems through chemical analyses on clinopyroxene - a look into the history of the Teno ankaramites, Tenerife. (45 hp)
596. Kryffin, Isidora, 2020: Kan benceller bevaras över miljontals år? (15 hp)
597. Halvarsson, Ellinor, 2020: Sökande efter nedslagskratrar i Sverige, med fokus på avtryck i berggrunden. (15 hp)
598. Jirdén, Elin, 2020: Kustprocesser i Arktis – med en fallstudie på Prins Karls Forland, Svalbard. (15 hp)
599. Chonewicz, Julia, 2020: The Eemian Baltic Sea hydrography and paleoenvironment based on foraminiferal geochemistry. (45 hp)
600. Paradeisis-Stathis, Savvas, 2020: Holocene lake-level changes in the Siljan Lake District – Towards validation of von Post’s drainage scenario. (45 hp)
601. Johansson, Adam, 2020: Groundwater flow modelling to address hydrogeological response of a contaminated site to remediation measures at Hjortsberga, southern Sweden. (15 hp)
602. Barrett, Aodhan, 2020: Major and trace element geochemical analysis of norites in the Hakefjorden Complex to constrain magma source and magma plumbing systems. (45 hp)
603. Lundqvist, Jennie, 2020: ”Man fyller det med information helt enkelt”: en fenomenografisk studie om studenters upplevelse av geologisk tid. (45 hp)
604. Zachén, Gabriel, 2020: Classification of four mesosiderites and implications for their formation. (45 hp)
605. Viðarsdóttir, Halla Margrét, 2020: Assessing the biodiversity crisis whitin the Triassic-Jurassic boundary interval using redox sensitive trace metals and stable carbon isotope geochemistry. (45 hp)
606. Tan, Brian, 2020: Nordvästra Skånes prekambriska geologiska utveckling. (15 hp)
607. Taxopoulou, Maria Eleni, 2020: Metamorphic micro-textures and mineral assemblages in orthogneisses in NW Skåne – how do they correlate with technical properties? (45 hp)
608. Damber, Maja, 2020: A palaeoecological study of the establishment of beech forest in Söderåsen National Park, southern Sweden. (45 hp)
609. Karastergios, Stylianos, 2020: Characterization of mineral parageneses and metamorphic textures in eclogite- to high-pressure granulite-facies marble at Allmenningen, Roan, western Norway. (45 hp)
610. Lindberg Skutsjö, Love, 2021: Geologiska och hydrogeologiska tolkningar av SkyTEM-data från Vombsänkan, Sjöbo kommun, Skåne. (15 hp)
611. Hertzman, Hanna, 2021: Odensjön - A new varved lake sediment record from southern Sweden. (45 hp)
612. Molin, Emmy, 2021: Rare terrestrial vertebrate remains from the Pliensbachian (Lower Jurassic) Hasle Formation on the Island of Bornholm, Denmark. (45 hp)
613. Höjbert, Karl, 2021: Dendrokronologi - en nyckelmetod för att förstå klimat- och miljöförändringar i Jämtland under holocen. (15 hp)
614. Lundgren Sassner, Lykke, 2021: A Method for Evaluating and Mapping Terrestrial Deposition and Preservation Potential- for Palaeostorm Surge Traces. Remote Mapping of the Coast of Scania, Blekinge and Halland, in Southern Sweden, with a Field Study at Dalköpinge Ängar, Trelleborg. (45 hp)
615. Granbom, Johanna, 2021: En detaljerad undersökning av den mellanordoviciska ”furudalkalkstenen” i Dalarna. (15 hp)
616. Greiff, Johannes, 2021: Oolites from the Arabian platform: Archives for the aftermath of the end-Triassic mass extinction. (45 hp)
617. Ekström, Christian, 2021: Rödfärgade utfällningar i dammanläggningar orsakade av *G. ferruginea* och *L. ochracea* - Problemstatistik och mikrobiella levnadsförutsättningar. (15 hp)
618. Östsjö, Martina, 2021: Geologins betydelse i samhället och ett första steg mot en geopark på Gotland. (15 hp)
619. Westberg, Märta, 2021: The preservation of cells in biomineralized vertebrate tissues of Mesozoic age – examples from a Cretaceous mosasaur (Reptilia, Mosasauridae). (45 hp)
620. Gleisner, Lovisa, 2021: En detaljerad undersökning av kalkstenslager i den mellanordoviciska gullhögenformationen på Billingen i Västergötland. (15 hp)
621. Bonnevier Wallstedt, Ida, 2021: Origin and early evolution of isopods - exploring morphology, ecology and systematics. (15 hp)
622. Selezeneva, Natalia, 2021: Indications for solar storms during the Last Glacial Maximum in the NGRIP ice core. (45 hp)
623. Bakker, Aron, 2021: Geological charac-

terisation of geophysical lineaments as part of the expanded site descriptive model around the planned repository site for high-level nuclear waste, Forsmark, Sweden. (45 hp)

624. Sundberg, Oskar, 2021: Jordlagerföljden i Höjeådalen utifrån nya borrningar. (15 hp)
625. Sartell, Anna, 2021: The igneous complex of Ekmanfjorden, Svalbard: an integrated field, petrological and geochemical study. (45 hp)
626. Juliusson, Oscar, 2021: Implications of ice-bedrock dynamics at Ullstorp, Scania, southern Sweden. (45 hp)
627. Eng, Simon, 2021: Rödslam i svenska kraftdammar - Problematik och potentiella lösningar. (15 hp)
628. Kervall, Hanna, 2021: Feasibility of Enhanced Geothermal Systems in the Precambrian crystalline basement in SW Scania, Sweden. (45 hp)
629. Smith, Thomas, 2022: Assessing the relationship between hypoxia and life on Earth, and implications for the search for habitable exoplanets. (45 hp)
630. Neumann, Daniel, 2022: En mosasaurie (Reptilia, Mosasauridae) av paleocensk ålder? (15 hp)
631. Svensson, David, 2022: Geofysisk och geologisk tolkning av kritskollors utbredning i Ystadsområdet. (15 hp)
632. Allison, Edward, 2022: Avsättning av Black Carbon i sediment från Odensjön, södra Sverige. (15 hp)
633. Jirdén, Elin, 2022: OSL dating of the Mesolithic site Nilsvikdalen 7, Bjorøy, Norway. (45 hp)
634. Wong, Danny, 2022: GIS-analys av effekten vid stormflod/havsnivåhöjning, Morupstrakten, Halland. (15 hp)
635. Lycke, Björn, 2022: Mikroplast i vattenavsatta sediment. (15 hp)
636. Schönherr, Lara, 2022: Grön fältspat i Varbergskomplexet. (15 hp)
637. Funck, Pontus, 2022: Granens ankomst och etablering i Skandinavien under postglacial tid. (15 hp)
638. Brotzen, Olga M., 2022: Geologiska besöksmål och geoparker som plattform för popularisering av geovetenskap. (15 hp)
639. Lodi, Giulia, 2022: A study of carbon, nitrogen, and biogenic silica concentrations in *Cyperus papyrus*, the sedge dominating the permanent swamp of the Okavango Delta, Botswana, Africa. (45 hp)
640. Nilsson, Sebastian, 2022: PFAS- En sammanfattning av ny forskning, med ett fokus på föroreningskällor, provtagning, analysmetoder och saneringsmetoder. (15 hp)
641. Jägfeldt, Hans, 2022: Molnens påverkan på jordens strålningsbalans och klimatsystem. (15 hp)
642. Sundberg, Melissa, 2022: Paleontologiska egenskaper och syreisotopsutveckling i borrkärnan Limhamn-2018: Kopplingar till klimatförändringar under yngre krita. (15 hp)
643. Bjermo, Tim, 2022: A re-investigation of hummocky moraine formed from ice sheet decay using geomorphological and sedimentological evidence in the Vomb area, southern Sweden. (45 hp)
644. Halvarsson, Ellinor, 2022: Structural investigation of ductile deformations across the Frontal Wedge south of Lake Vättern, southern Sweden. (45 hp)
645. Brakebusch, Linus, 2022: Record of the end-Triassic mass extinction in shallow marine carbonates: the Lorüns section (Austria). (45 hp)
646. Wahlquist, Per, 2023: Stratigraphy and palaeoenvironment of the early Jurassic volcaniclastic strata at Djupadalsmölla, central Skåne, Sweden. (45 hp)
647. Gebremedhin, G. Gebreselassie, 2023: U-Pb geochronology of brittle deformation using LA-ICP-MS imaging on calcite veins. (45 hp)
648. Mroczek, Robert, 2023: Petrography of impactites from the Dellen impact structure, Sweden. (45 hp)
649. Gunnarsson, Niklas, 2023: Upper Ordovician stratigraphy of the Stora Sutarve core (Gotland, Sweden) and an assessment of the Hirnantian Isotope Carbon Excursion (HICE) in high-resolution. (45 hp)

LUNDS UNIVERSITET

**Geologiska institutionen**
**Lunds universitet**
**Sölvegatan 12, 223 62 Lund**